

# Large Scale Model Predictive Control with Neural Networks and Primal Active Sets <sup>★</sup>

Steven W. Chen <sup>a</sup>, Tianyu Wang <sup>b</sup>, Nikolay Atanasov <sup>b</sup>, Vijay Kumar <sup>a</sup>,  
Manfred Morari <sup>a</sup>

<sup>a</sup>University of Pennsylvania, GRASP Laboratory, Philadelphia, PA

<sup>b</sup>University of California, San Diego, La Jolla, CA

---

## Abstract

This work presents an explicit-implicit procedure that combines an offline trained neural network with an online primal active set solver to compute a model predictive control (MPC) law with guarantees on recursive feasibility and asymptotic stability. The neural network improves the suboptimality of the controller performance and accelerates online inference speed for large systems, while the primal active set method provides corrective steps to ensure feasibility and stability. We highlight the connections between MPC and neural networks and introduce a primal-dual loss function to train a neural network to initialize the online controller. We then demonstrate online computation of the primal feasibility and suboptimality criteria to provide the desired guarantees. Next, we use these neural network and criteria measures to accelerate an online primal active set method through warm starts and early termination. Finally, we present a data set generation algorithm that is critical for successfully applying our approach to high dimensional systems. The primary motivation is developing an algorithm that scales to systems that are challenging for current approaches, involving state and input dimensions as well as planning horizons in the order of tens to hundreds.

*Key words:* Neural Network; Model Predictive Control; Receding Horizon Control.

---

## 1 Introduction

Model predictive control (MPC) is a dynamic optimization technique widely used in industrial process applications such as oil refineries and chemical plants [29]. Recently, MPC has found mainstream use in robotics for the control of ground [30], aerial [6, 38], and humanoid [9] robots due to its versatility, robustness, and safety guarantees. The transition from the process industry to robotics brings additional challenges since the computation time is reduced from hours to milliseconds.

MPC techniques can be categorized into implicit and explicit MPC. Implicit MPC focuses on efficient online

computation of an open-loop control sequence, optimizing the system performance at its current state. Wang and Boyd [37] exploit the MPC problem structure to design an interior point method that decreases the time complexity of solving the associated quadratic program (QP). Vichik and Borelli [36] experiment with an entirely different computation scheme and demonstrate that analog circuits can solve QPs in microseconds, but require custom hardware.

Rather than solving an optimization problem online, explicit methods manage the computational load by pre-computing the optimal control law  $\mathbf{u}^* = \boldsymbol{\mu}^*(\mathbf{x})$  offline as a function of all feasible states  $\mathbf{x}$ , where the optimal control is known to be piecewise affine on polytopes. The drawback of explicit MPC approaches is that the computational complexity, measured by the number of polytopic regions, grows quickly with the number of constraints. As a result, computing the optimal explicit control law can become computationally intractable for large systems. In addition, even if this optimal control law can be computed, the process of determining which region contains the system state can require too much

---

<sup>★</sup> This paper was not presented at any IFAC meeting. Corresponding author S. W. Chen. Tel. +XXXIX-VI-mmmxxi. Fax +XXXIX-VI-mmmxxv.

*Email addresses:* chenste@seas.upenn.edu (Steven W. Chen), tiw161@eng.ucsd.edu (Tianyu Wang), natanasov@eng.ucsd.edu (Nikolay Atanasov), kumar@seas.upenn.edu (Vijay Kumar), morari@seas.upenn.edu (Manfred Morari).

processing power or memory storage for real-time execution [23].

One approach to address the computational limitations of optimal explicit MPC control laws is to compute an approximate sub-optimal controller. Jones and Morari [19] use a double-description method to build piecewise affine (PWA) approximations of the value function, and use barycentric functions on the polytopic regions of the approximate value function to compute an approximate control law. In addition, they are able to prove recursive feasibility and asymptotic stability of the suboptimal controller. These approaches, however, have not been demonstrated to scale to the same problem sizes as those handled by implicit MPC methods.

A promising approach that this paper investigates is the use of a neural network to approximate the MPC control law. There have been several recent works using neural network architectures for MPC design. Chen et al. [8] use a neural network with an orthogonal projection operation to approximate the optimal control law. Hertneck et al. [15] use a neural network in a robust MPC framework to provide statistical guarantees of feasibility and stability. Zhang et al. [41] use a neural network to approximate the primal and dual variables, and provide statistical guarantees as well as certificates of sub-optimality. Our work extends these approaches by providing non-statistical guarantees on recursive feasibility and asymptotic stability through the integration with an online solver. Moreover, we demonstrate for the first time that neural-network based approximations of MPC control laws can scale to very large systems.

A few closely related works combine the strengths of machine learning for scalability with the analytical tractability of QP problems in an explicit-implicit MPC approach. Zeilinger et al. [40] compute a piecewise affine approximation of the optimal control law, combine it with an active set method, and provide criteria to terminate the active set method early while still obtaining guarantees on recursive feasibility and asymptotic stability. Klaučo et al. [22] use classification trees and nearest neighbors to warm start an active set method and solve to the optimal solution. These approaches differ from our method because they do not utilize a neural network as the function approximator, and do not demonstrate the ability to scale to large systems.

The challenge of generating a large training data set containing the initial feasible states and their corresponding optimal inputs, primal variables, or dual variables for high-dimensional systems has not been widely studied in the MPC literature. Yet, generating such data is critical for scaling any learning-based explicit MPC approach to high dimensions because a naive approach would waste large amounts of computation to obtain feasible initial states. Current work either does not address this problem, uses gridding [22, 33] or random sampling [15, 41]

methods that cannot scale to high dimensions, or relies on reinforcement and imitation learning techniques that perform closed-loop simulations leading to weaknesses discussed in [31]. Our work proposes an algorithm to efficiently generate large datasets in high dimensions based on theory from *geometric random walks* and *quasi Monte Carlo (QMC)* sequences.

In summary, the goal of this work is to develop a neural-network-based suboptimal MPC control law that can scale to large system sizes, reduce online computation time relative to implicit methods, and provide guarantees on recursive feasibility and asymptotic stability. Specifically, our contributions include:

- a primal-dual loss function that incorporates state and input constraints to train a neural network approximation of explicit MPC control law;
- a control law that corrects the network output using a primal active set solver and terminates early once necessary criteria for recursive feasibility and asymptotic stability have been reached;
- a data set generation algorithm utilizing ideas from geometric random walks that efficiently generates feasible samples for large systems; and
- a demonstration that the proposed approach scales to large problems with 36 states, 9 inputs, and time horizon of 50.

## 2 Problem Statement

Consider a discrete-time linear time-invariant system,

$$\mathbf{x}(t+1) = \mathbf{A}\mathbf{x}(t) + \mathbf{B}\mathbf{u}(t), \quad (1)$$

subject to a set of constraints,

$$\begin{aligned} \mathbf{x}(t) \in \mathcal{X} &:= \{\mathbf{x} \in \mathbb{R}^n \mid \mathbf{A}_x \mathbf{x} \leq \mathbf{b}_x\} & \forall t \geq 0, \\ \mathbf{u}(t) \in \mathcal{U} &:= \{\mathbf{u} \in \mathbb{R}^m \mid \mathbf{A}_u \mathbf{u} \leq \mathbf{b}_u\} & \forall t \geq 0. \end{aligned} \quad (2)$$

Assume that the pair  $(\mathbf{A}, \mathbf{B})$  is stabilizable. For a given state  $\mathbf{x}(0)$ , our goal is to compute a sequence of control inputs  $\mathbf{u}_{0:\infty} := \{\mathbf{u}_0, \mathbf{u}_1, \dots\}$  to regulate the system to a desired state in the interior of the feasible set (2). Without loss of generality, this desired state will be assumed to be the origin. This problem, known as the constrained infinite-horizon LQR problem, is:

$$\begin{aligned} \arg \min_{\mathbf{u}_{0:\infty}} \quad & J_\infty(\mathbf{x}(0)) = \sum_{k=0}^{\infty} (\mathbf{x}_k^T \mathbf{Q} \mathbf{x}_k + \mathbf{u}_k^T \mathbf{R} \mathbf{u}_k) \\ \text{s.t.} \quad & \mathbf{x}_{k+1} = \mathbf{A} \mathbf{x}_k + \mathbf{B} \mathbf{u}_k, \quad \mathbf{x}_0 = \mathbf{x}(0), \\ & \mathbf{A}_x \mathbf{x}_k \leq \mathbf{b}_x, \\ & \mathbf{A}_u \mathbf{u}_k \leq \mathbf{b}_u, \end{aligned} \quad (3)$$

where  $\mathbf{Q} \in \mathcal{S}_{>0}^n$  and  $\mathbf{R} \in \mathcal{S}_{>0}^m$  are chosen to define the desired optimal behavior for the system. When optimal

behavior is needed at multiple initial states, instead of recomputing the input sequence  $\mathbf{u}_{0:\infty}$  every time, it is desirable to obtain a control policy  $\boldsymbol{\mu}^*(\mathbf{x})$  that specifies the optimal input for an arbitrary state  $\mathbf{x}$ .

### 3 Preliminaries

#### 3.1 Model Predictive Control Formulation

*Receding horizon control* (RHC) obtains a suboptimal controller for Problem (3) by repeatedly solving the following finite-horizon problem:

$$\begin{aligned} \arg \min_{\mathbf{u}_{0:N-1}} \quad & J(\mathbf{u}_{0:N-1}|\mathbf{x}(t)) = \mathbf{x}_N^T \mathbf{P} \mathbf{x}_N \\ & + \sum_{k=0}^{N-1} (\mathbf{x}_k^T \mathbf{Q} \mathbf{x}_k + \mathbf{u}_k^T \mathbf{R} \mathbf{u}_k) \\ \text{s.t.} \quad & \mathbf{x}_{k+1} = \mathbf{A} \mathbf{x}_k + \mathbf{B} \mathbf{u}_k, \quad \mathbf{x}_0 = \mathbf{x}(t), \\ & \mathbf{A}_x \mathbf{x}_k \leq \mathbf{b}_x, \\ & \mathbf{A}_u \mathbf{u}_k \leq \mathbf{b}_u, \\ & \mathbf{A}_f \mathbf{x}_N \leq \mathbf{b}_f, \end{aligned} \quad (4)$$

where  $N$  is the horizon,  $\mathbf{x}_k$  is a prediction of the state at  $t+k$  and is an *optimization* variable, while  $\mathbf{x}(t)$  is the actual state at the current time  $t$  and is a *parameter*. Note that a terminal cost,  $\mathbf{x}_N^T \mathbf{P} \mathbf{x}_N$ , that bounds the cost for the remaining time  $N, \dots, \infty$  and a terminal constraint set,  $\mathcal{X}_f := \{\mathbf{x} \in \mathbb{R}^n | \mathbf{A}_f \mathbf{x} \leq \mathbf{b}_f\}$ , have been added to the problem to ensure feasibility and asymptotic stability of the receding horizon controller as will be discussed in Sec. 3.3. In the following, we drop the time  $t$  to simplify notation. The batch formulation of (4) is:

$$\begin{aligned} \underset{\mathbf{z}}{\text{argmin}} \quad & J(\mathbf{z}|\mathbf{x}) = \mathbf{z}^T \mathbf{H} \mathbf{z} + \mathbf{x}^T \mathbf{Q} \mathbf{x} \\ \text{s.t.} \quad & \mathbf{G}_{\text{eq}} \mathbf{z} = \mathbf{E}_{\text{eq}} \mathbf{x} \\ & \mathbf{G}_{\text{in}} \mathbf{z} \leq \mathbf{w}_{\text{in}} + \mathbf{E}_{\text{in}} \mathbf{x} \end{aligned} \quad (5)$$

with the following definitions

$$\begin{aligned} \mathbf{z} &= [\mathbf{x}_1^T \dots \mathbf{x}_N^T \mathbf{u}_0^T \dots \mathbf{u}_{N-1}^T] \in \mathbb{R}^{N(n+m)} \\ \mathbf{H} &= \text{diag}(\mathbf{I}_{N-1} \otimes \mathbf{Q}, \mathbf{P}, \mathbf{I}_N \otimes \mathbf{R}) \in \mathbb{R}^{N(n+m) \times N(n+m)} \\ \mathbf{G}_{\text{eq}} &= [\mathbf{I}_{Nn} - \mathbf{L}_N \otimes \mathbf{A}; -\mathbf{I}_N \otimes \mathbf{B}] \in \mathbb{R}^{Nn \times N(n+m)} \\ \mathbf{E}_{\text{eq}} &= \mathbf{e}_1 \otimes \mathbf{A} \in \mathbb{R}^{Nn \times n} \\ \mathbf{G}_{\text{in}} &= \text{diag}(\mathbf{0}_{c_x}, \mathbf{I}_{N-1} \otimes \mathbf{A}_x, \mathbf{A}_f, \mathbf{I}_N \otimes \mathbf{A}_u) \\ \mathbf{E}_{\text{in}} &= -\mathbf{e}_1 \otimes \mathbf{A}_x \in \mathbb{R}^{(Nc_x + c_f + Nc_u) \times n} \\ \mathbf{w}_{\text{in}} &= [\mathbf{1}_N \otimes \mathbf{b}_x; \mathbf{b}_f; \mathbf{1}_N \otimes \mathbf{b}_u] \in \mathbb{R}^{(Nc_x + c_f + Nc_u)} \end{aligned} \quad (6)$$

where  $\mathbf{L}_N$  is the matrix of size  $N \times N$  with ones on the first subdiagonal and zeros elsewhere,  $\mathbf{e}_i$  is the  $i$ -th standard basis vector,  $\mathbf{1}_N$  is the vector of all ones of size  $N$ ,  $c_x, c_f, c_u$  denote the number of constraints specified by

the rows of  $\mathbf{A}_x, \mathbf{A}_f, \mathbf{A}_u$ , respectively, “;” denotes the vertical concatenation operation, and  $\otimes$  denotes the Kronecker product. When the parameter  $\mathbf{x}$  is fixed, Problem (5) is a *quadratic program* (QP) and the solution is a vector  $\mathbf{z}$ .

A common choice for the terminal cost matrix  $\mathbf{P}$  is the solution to the Algebraic Riccati Equation:

$$\mathbf{P}_\infty = \mathbf{A}^T \mathbf{P}_\infty \mathbf{A} + \mathbf{Q} - \mathbf{A}^T \mathbf{P}_\infty \mathbf{B} (\mathbf{B}^T \mathbf{P}_\infty \mathbf{B} + \mathbf{R})^{-1} \mathbf{B}^T \mathbf{P}_\infty \mathbf{A} \quad (7)$$

which corresponds to the optimal cost-to-go of an unconstrained infinite-horizon LQR problem. With this choice of terminal cost and a large enough  $N$ , solving the finite-horizon problem (4) will actually yield the optimal solution to the infinite-horizon problem (3) [4]. A common choice for  $\mathcal{X}_f$  is the region is the maximal positively invariant set of the LQR controller  $\mathcal{O}_\infty^{\text{LQR}}$ , which is computable via reachability analysis [5, Ch.11].

**System 1 (Double Integrator)** Throughout the paper, we will use the 2-D double integrator system,

$$\mathbf{x} \in \mathbb{R}^2, \quad \mathbf{u} \in \mathbb{R}, \quad \mathbf{A} = \begin{bmatrix} 1 & 0.1 \\ 0 & 1 \end{bmatrix}, \quad \mathbf{B} = \begin{bmatrix} 0.005 \\ 0.1 \end{bmatrix},$$

to illustrate various concepts. We are interested in stabilizing the system by solving (3) with cost terms  $\mathbf{Q} = \mathbf{I}_2, \mathbf{R} = 1$ , subject to position and velocity constraints,  $\mathbf{A}_x = [\mathbf{I} \ -\mathbf{I}]^T, \mathbf{b}_x = [5 \ 1 \ 5 \ 1]^T$ , and input constraints  $|u_k| \leq 2$ , for  $k = 1, \dots, \infty$ . We consider the RHC formulation in (4) with a planning horizon  $N = 10$ . We choose the terminal region  $\mathcal{X}_f$  to be  $\mathcal{O}_\infty^{\text{LQR}}$ , and the terminal cost  $\mathbf{x}_N^T \mathbf{P}_\infty \mathbf{x}_N$ . The constraint sizes are  $c_x = 4, c_f = 6$ , and  $c_u = 2$ . The primal variables have dimension 30, the dual variables corresponding to the inequality constraints have dimension 66, and the dual variables corresponding to the equality constraints have dimension 20.

#### 3.2 Feasibility and Duality

For a given state parameter  $\mathbf{x}$ , QP (5) is a strictly convex QP because the matrix  $\mathbf{H}$  is positive definite. A decision variable  $\mathbf{z}$  is called *primal feasible* for a parameter  $\mathbf{x}$  if  $\mathbf{G}_{\text{eq}} \mathbf{z} = \mathbf{E}_{\text{eq}} \mathbf{x}$  and  $\mathbf{G}_{\text{in}} \mathbf{z} \leq \mathbf{w}_{\text{in}} + \mathbf{E}_{\text{in}} \mathbf{x}$ .

Let  $\mathcal{X}_0 \subseteq \mathcal{X}$  be the set of parameters  $\mathbf{x}$  for which QP (5) is feasible [5, Defn. 6.3]. The set  $\mathcal{X}_0$  is a polyhedron but is difficult to compute because it requires expensive polyhedral projections or recursive backward reachable set computations [5, Ch. 6 and 11]. Given  $\mathbf{x} \in \mathcal{X}_0$  and an associated primal feasible  $\mathbf{z}$ , the *suboptimality level* of  $\mathbf{z}$  is:

$$\sigma(\mathbf{z}|\mathbf{x}) := J(\mathbf{z}|\mathbf{x}) - J(\mathbf{z}^*|\mathbf{x}) \geq 0 \quad (8)$$

where  $\mathbf{z}^*$  is the unique minimizer (due to strict convexity) of QP (5). A common technique to handle the constraints in QP (5) is to use duality theory and introduce

dual variables  $(\boldsymbol{\nu}, \boldsymbol{\lambda})$  [7, Ch.5]. Define the Lagrangian associated with QP (5) as:

$$\mathcal{L}(\mathbf{z}, \boldsymbol{\nu}, \boldsymbol{\lambda}|\mathbf{x}) := \mathbf{z}^T \mathbf{H} \mathbf{z} + \mathbf{x}^T \mathbf{Q} \mathbf{x} + \boldsymbol{\nu}^T (\mathbf{G}_{\text{eq}} \mathbf{z} - \mathbf{E}_{\text{eq}} \mathbf{x}) + \boldsymbol{\lambda}^T (\mathbf{G}_{\text{in}} \mathbf{z} - \mathbf{w}_{\text{in}} - \mathbf{E}_{\text{in}} \mathbf{x}). \quad (9)$$

The Lagrangian dual of a minimization QP is a maximization QP over the variables  $(\boldsymbol{\nu}, \boldsymbol{\lambda})$  with the following objective function:

$$d(\boldsymbol{\nu}, \boldsymbol{\lambda}|\mathbf{x}) = \inf_{\mathbf{z}} \mathcal{L}(\mathbf{z}, \boldsymbol{\nu}, \boldsymbol{\lambda}|\mathbf{x}), \quad (10)$$

where the minimization over  $\mathbf{z}$  can be done in closed-form for a convex QP. The dual variables  $(\boldsymbol{\nu}, \boldsymbol{\lambda})$  are called *dual feasible* if  $\boldsymbol{\lambda} \geq 0$ . For a given parameter  $\mathbf{x}$ , any primal feasible  $\mathbf{z}$ , any dual feasible  $(\boldsymbol{\nu}, \boldsymbol{\lambda})$ , and optimal primal-dual variables  $(\mathbf{z}^*, \boldsymbol{\nu}^*, \boldsymbol{\lambda}^*)$ , *strong duality* holds because Slater's conditions are satisfied [7, Ch.5]:

$$d(\boldsymbol{\nu}, \boldsymbol{\lambda}|\mathbf{x}) \leq d(\boldsymbol{\nu}^*, \boldsymbol{\lambda}^*|\mathbf{x}) = \mathcal{L}(\mathbf{z}^*, \boldsymbol{\nu}^*, \boldsymbol{\lambda}^*|\mathbf{x}) = J(\mathbf{z}^*|\mathbf{x}) \leq J(\mathbf{z}|\mathbf{x}). \quad (11)$$

Finally, define the *feasible duality gap* associated with  $\mathbf{x}$ ,  $\mathbf{z}$ ,  $\boldsymbol{\nu}$ ,  $\boldsymbol{\lambda}$  as

$$\eta(\mathbf{z}, \boldsymbol{\nu}, \boldsymbol{\lambda}|\mathbf{x}) := J(\mathbf{z}|\mathbf{x}) - d(\boldsymbol{\nu}, \boldsymbol{\lambda}|\mathbf{x}) \geq \sigma(\mathbf{z}|\mathbf{x}) \geq 0 \quad (12)$$

which is an upper bound on the suboptimality level  $\sigma(\mathbf{z}|\mathbf{x})$  for any feasible  $(\mathbf{z}, \boldsymbol{\nu}, \boldsymbol{\lambda})$  due to Eqn. (11).

### 3.3 Receding Horizon Control

Fixing the state parameter  $\mathbf{x}$  yields QP (5) that minimizes over a vector of primal variables  $\mathbf{z}$ . We can instead view the analog, the *multiparametric quadratic program* (mp-QP) that minimizes over functions that map  $\mathbf{x}$  to  $\mathbf{z}$  [5, Ch. 6].

**Definition 1 (Planner)** *A planner is a function  $\pi : \mathcal{X}_0 \rightarrow \mathbb{R}^{N(n+m)}$  that maps a parameter  $\mathbf{x}$  to a decision variable  $\mathbf{z}$ . A planner  $\pi$  is primal feasible if  $\mathbf{z} = \pi(\mathbf{x})$  is a primal feasible variable for QP (5)  $\forall \mathbf{x} \in \mathcal{X}_0$ . It is optimal if  $\mathbf{z} = \pi(\mathbf{x})$  is the optimal solution  $\forall \mathbf{x} \in \mathcal{X}_0$ .*

The following definitions show how a planner  $\pi$  can be implemented as a receding horizon controller (RHC)  $\mu$ .

#### Definition 2 (Closed Loop System and RHC)

*Let  $\pi$  be a planner. Let  $\mu : \mathcal{X}_0 \rightarrow \mathbb{R}^m$  denote the first control input  $\mathbf{u}_0$  in  $\mathbf{z} = \pi(\mathbf{x})$ , that is  $\mathbf{u}_0 = \mu(\mathbf{x})$ . Define the closed loop system*

$$\mathbf{x}(t+1) = \mathbf{A}\mathbf{x}(t) + \mathbf{B}\mu(\mathbf{x}(t)) = f_{\text{cl}}(\mathbf{x}(t)), \quad t \geq 0.$$

$\mu$  is known as the RHC corresponding to the planner  $\pi$ .

There are two desirable properties that we would like to guarantee for our control law, which we define below.

**Definition 3 (Recursive Feasibility)** *The RHC  $\mu$  is recursively feasible if  $\mathbf{x}(t) \in \mathcal{X}_0 \implies \mathbf{x}(t+1) = f_{\text{cl}}(\mathbf{x}(t)) \in \mathcal{X}_0 \forall t \geq 0$ .*

Primal feasibility is a property of the planner and open loop optimization problem, while recursive feasibility is a property of the RHC and corresponding closed loop system. In general, primal feasibility of the open loop optimization problem does not imply recursive feasibility of the corresponding closed loop controller. We next define the notion of stability around an equilibrium point.

**Definition 4 (Equilibrium Point)** *A point  $\bar{\mathbf{x}} \in \mathcal{X}_0$  is called an equilibrium point if  $\mathbf{x}(t+1) = f_{\text{cl}}(\mathbf{x}(t)) = \bar{\mathbf{x}} \forall t = 0, 1, 2, \dots$ .*

**Definition 5 (Asymptotic Stability)** *The equilibrium point  $\bar{\mathbf{x}}$  is stable if  $\forall \epsilon > 0, \exists \delta(\epsilon) > 0$  such that  $\|\mathbf{x}(0) - \bar{\mathbf{x}}\| < \delta \implies \|\mathbf{x}(t) - \bar{\mathbf{x}}\| < \epsilon, \forall t \geq 0$ .*

*In addition,  $\bar{\mathbf{x}}$  is asymptotically stable if it is stable and  $\delta$  can be chosen such that*

$$\|\mathbf{x}(0) - \bar{\mathbf{x}}\| < \delta \implies \lim_{t \rightarrow \infty} \mathbf{x}(t) = \bar{\mathbf{x}}.$$

Recursive feasibility of a control law is a necessary, but not sufficient, condition for asymptotic stability.

## 4 Technical Approach and Overview

Our primary motivation is learning a controller with guarantees for high-dimensional problems with large state and input dimensions and long time horizons. Large problems are challenging since traditional explicit MPC approaches become too computationally expensive, and even implicit MPC may require custom architectures on FPGAs for real-time inference [17]. We propose a hybrid explicit-implicit procedure that merges an offline trained neural network with an online primal active set solver to compute a planner  $\pi$ . The neural network approximation of the planner enables our procedure to scale to these large problems. The primal active set solver then provides a few corrective steps to meet the conditions necessary to guarantee recursive feasibility and asymptotic stability.

In Sec. 5, we describe the offline neural network architecture training procedure. The neural network approximates a planner  $\tilde{\pi}$  by mapping the state  $\mathbf{x}$  to a primal prediction  $\tilde{\mathbf{z}}$ . We highlight the connections between neural networks with rectified linear unit (ReLU) activation functions and the optimal planner and RHC for MPC problems. We then introduce a primal-dual loss function

based on the Lagrangian function to train the neural network.

In Sec. 6, we describe the conditions necessary to obtain guarantees of recursive feasibility and asymptotic stability of the RHC  $\mu$  corresponding to an optimal and suboptimal planner  $\pi$ . These conditions center on both checking for primal feasibility and bounding the suboptimality of the planner. We then introduce a procedure to obtain certificates of primal feasibility and suboptimality for a given state parameter  $\mathbf{x}$  and the primal variable  $\mathbf{z}$ , without the need of additional inputs such as the dual variables  $\boldsymbol{\nu}, \boldsymbol{\lambda}$ .

In Sec. 7, we introduce primal active set methods. We describe how to merge these methods with the neural network in a manner that reduces the extra necessary online computation. The combination computes a new suboptimal planner  $\hat{\pi}$  that yields a RHC  $\hat{\mu}$  that is recursively feasible and asymptotically stable.

In Sec. 8, we highlight the practical issues that arise when scaling the proposed procedure to high dimensional problems. The main challenge is drawing samples from the domain of our planner  $\mathcal{X}_0$  to train and evaluate the neural network, as  $\mathcal{X}_0$  is difficult to compute for large problems. Instead we have a *membership oracle* in the form of a QP solver that given a state parameter  $\mathbf{x}$ , will determine whether the corresponding QP (5) has a solution. We demonstrate how standard sampling methods such as gridding or Monte Carlo rejection sampling will not scale to high dimensions, and introduce the theory of *geometric random walks* to surpass this problem. We then develop a practical method motivated by this theory to generate large datasets for large scale problems.

In Sec. 9, we present results and analysis on four systems that demonstrate the ability of our proposed approach to scale to large systems. We also provide illustrative metrics that highlight the encountered challenges that shaped the development of this method. The largest problem we analyze has 36 states, 9 inputs, and time horizon of 50, and our results indicate that our method can be applied to even larger systems. We did not analyze a larger system since the implementation we used to generate Sobol sequences (described in Sec. 8) was limited to 40 dimensions.

## 5 Offline Neural Network Training

The first step of our approach is offline training of a deep neural network  $\phi(\mathbf{x}|\boldsymbol{\theta})$  that provides a candidate solution  $\bar{\mathbf{z}}$  for the QP optimization in (5). We choose to approximate the entire primal prediction over the planning horizon instead of the control law  $\mu$ . Although this choice requires approximating  $N(n+m)$  variables compared to only  $m$ , these additional predicted variables are

used to obtain the desired guarantees through the online primal active set solver.

**Definition 6** (*Deep Neural Network*) A deep neural network (DNN)  $\phi(\mathbf{x}|\boldsymbol{\theta})$  with  $L$  layers is a composition of  $L$  affine functions

$$\boldsymbol{\lambda}_j(\mathbf{x}) := \boldsymbol{\theta}_j^W \mathbf{x} + \boldsymbol{\theta}_j^b, \quad (13)$$

each except the last one followed by a nonlinear activation function  $\mathbf{h}$ , so that:

$$\phi(\mathbf{x}|\boldsymbol{\theta}) = \boldsymbol{\lambda}_L \circ \mathbf{h} \circ \boldsymbol{\lambda}_{L-1} \circ \dots \circ \mathbf{h} \circ \boldsymbol{\lambda}_1(\mathbf{x}),$$

where  $\boldsymbol{\theta} := \{(\boldsymbol{\theta}_j^W, \boldsymbol{\theta}_j^b)\}_{j=1}^L$  are the affine function parameters to be optimized, and  $\mathbf{h}$  is a fixed (not optimized) function, typically chosen as a sigmoid, hypertangent, or ReLu function (see [12, Ch.6] for details). The depth of the DNN is the number of layers  $L$ , and each layer  $l$  has a width defined by the number of rows of  $\boldsymbol{\theta}_l^W$  and  $\boldsymbol{\theta}_l^b$ .

The ReLu activation function is  $\mathbf{h}(\mathbf{x}) := \max\{\mathbf{0}, \mathbf{x}\}$ , where the max operation is applied elementwise. We restrict our search for a planner  $\pi$  within the class of functions computed by a ReLu DNN  $\phi$ . The goal is to design the architecture of  $\phi$ , and then search for parameters  $\boldsymbol{\theta}$  to approximate the optimal planner  $\phi(\mathbf{x}|\boldsymbol{\theta}) = \hat{\pi}(\mathbf{x}) \approx \pi^*(\mathbf{x}) \forall \mathbf{x} \in \mathcal{X}_0$ .

### 5.1 Piecewise Affine Neural Networks

We show that there exists a ReLu DNN architecture and corresponding network parameters that can represent the optimal planner  $\pi^*(\mathbf{x})$  for the mp-QP in (5) exactly. This justifies our choice to restrict the planner representation to a ReLu DNN. The solution to an mp-QP is continuous and piecewise-affine on polyhedra [5, Thm. 6.7]. In addition, this solution is unique due to the positive definiteness of  $\mathbf{H}$ . As a result,  $\pi^*$  is a unique, continuous, and piecewise-affine function on polyhedra. ReLu DNNs also represent continuous and piecewise-affine functions on polyhedra [3]. These observations allow us to establish the following connection between a ReLu DNN and the solution to an mp-QP.

**Theorem 7** (*Exact Representation*) Suppose  $f : \mathbb{R}^n \rightarrow \mathbb{R}^m$  for  $n, m \in \mathbb{N}^+$  is a continuous and piecewise-affine function on polyhedra. Then,  $f$  can be represented exactly by a ReLu DNN with depth at most

$$L = \lceil \log_2(n+1) \rceil + 1. \quad (14)$$

**PROOF.** Follows directly from [3, Thm. 2.1] which states the above result for  $m = 1$ . Generalizing to  $m > 1$  is trivial as we can take  $m$  such neural networks to represent the individual output dimensions, each bounded with the depth  $L$ .

Thm. 7 provides a guideline for choosing an appropriate network depth to approximate the planner  $\pi^*$  for a system with  $n$  states. For example, a neural network architecture approximating  $\pi^*$  for the double integrator system (Sys. 1) should have depth greater than 3.

Specifying an appropriate network architecture also requires a choice on the widths of each layer. It is possible to use ideas from [8] that connect additional ReLU DNN theory from [27], [3], [13] with mp-QP problems. These ideas provide valuable intuition on bounding the maximum number of regions representable by various architectures, but do not offer constructive procedures. As a result, we choose a network depth according to Thm. 7, and then use grid search to choose appropriate widths.

## 5.2 Neural Network Training

After designing the neural network architecture, the next step is to optimize the neural network parameters  $\theta$  to approximate  $\phi(\mathbf{x}|\theta) = \tilde{\pi}(\mathbf{x}) \approx \pi^*(\mathbf{x})$ . We rely on a training data set  $\mathcal{D}$  (supervised learning) to minimize a loss function over  $\theta$ . Since the neural network outputs the primal variables  $\mathbf{z}$ , a natural choice would be to use a dataset  $\mathcal{D} := \{(\mathbf{x}_i, \mathbf{z}_i^*)\}$  to optimize the primal least-squares loss function:

$$\sum_{i=1}^{|\mathcal{D}|} (\phi(\mathbf{x}_i|\theta) - \mathbf{z}_i^*)^2. \quad (15)$$

While this approach is reasonable, a more accurate estimate of the optimal planner  $\pi^*$  may be obtained by minimizing the suboptimality level defined in Eqn. (8). Using the same dataset  $\mathcal{D} := \{(\mathbf{x}_i, \mathbf{z}_i^*)\}$ , the ideal loss function would be:

$$\sum_{i=1}^{|\mathcal{D}|} [\sigma(\phi(\mathbf{x}_i|\theta)|\mathbf{x}_i)]^2 \quad (16)$$

s.t.  $\phi(\mathbf{x}_i|\theta)$  is primal feasible  $\forall i \leq |\mathcal{D}|$ ,

which includes a primal feasibility constraint on the neural network output. Including the primal feasibility constraint is necessary as there are potentially multiple infeasible primal variables  $\tilde{\mathbf{z}}$ , where  $J(\tilde{\mathbf{z}}|\mathbf{x}) \leq J(\mathbf{z}^*|\mathbf{x})$  and  $\sigma(\tilde{\mathbf{z}}|\mathbf{x}) \leq 0$ . The primal variables that minimize the suboptimality level and obey Eqn. (8) are unique only when we include the constraint of primal feasibility. However, minimizing Eqn. (16) is a constrained optimization problem that is difficult to minimize directly.

These challenges motivate a primal-dual loss function based on the Lagrangian (9) associated with QP (5). Assuming access to optimal dual variables, the data set format is now augmented to be  $\mathcal{D} := \{(\mathbf{x}_i, \mathbf{z}_i^*, \nu_i^*, \lambda_i^*)\}$ , and the loss function is:

$$\sum_{i=1}^{|\mathcal{D}|} (\mathcal{L}(\phi(\mathbf{x}_i|\theta), \nu_i^*, \lambda_i^*|\mathbf{x}_i) - \mathcal{L}(\mathbf{z}_i^*, \nu_i^*, \lambda_i^*|\mathbf{x}_i))^2. \quad (17)$$

The dual variables in both the predicted and optimal Lagrangian are the optimal dual variables  $(\nu_i^*, \lambda_i^*)$ . By strong duality in Eqn. (11), the unique minimizers are the optimal primal variables  $\mathbf{z}_i^*$ . As a result, minimizing Eqn. (17) minimizes the original Eqn. (16). Although this loss function requires storing more information in the data set  $\mathcal{D}$ , there is no additional computation necessary as both the optimal primal and dual variables are calculated by a QP solver when generating the dataset. The least squares Lagrangian loss in Eqn. (17) thus has the strengths of both the primal least squares loss in Eqn. (15) and the ideal suboptimal loss in Eqn. (16) as it is an unconstrained minimization problem that is still based on the QP cost matrices.

With the loss function designed in Eqn. (17), we use a standard stochastic gradient-based optimization techniques such as *Adam* [21] or *RMSProp* [34]. These approaches train the network by sampling a subset of the training dataset (mini-batch), computing the loss in Eqn. (17) over the mini-batch instead of the entire dataset, and then use backpropagation to compute the loss gradient to update the neural network parameters  $\theta$ . This sampling is continued until the dataset is exhausted, which concludes an epoch, and is then repeated until convergence.

## 6 Conditions and Certificates

The trained neural network  $\phi(\mathbf{x}|\theta)$  represents an approximate planner  $\tilde{\pi}$  that maps states  $\mathbf{x}$  to primal predictions  $\tilde{\mathbf{z}}$ . As a result, it can be implemented as a RHC  $\tilde{\mu}$  by efficiently recomputing  $\tilde{\mathbf{z}}$  using  $\phi(\mathbf{x}|\theta)$  and applying the corresponding first control input  $\tilde{\mathbf{u}}_0$  at each encountered state. We would like to guarantee recursive feasibility and asymptotic stability of this RHC. There are a few criteria that the planner has to satisfy in order to guarantee these properties.

### 6.1 Optimal RHC

We first analyze the conditions necessary to guarantee feasibility and stability of the optimal RHC. Recall that with a large enough  $N$  and proper choice of terminal cost, solving the finite-horizon problem (4) yields the solution to the infinite-horizon LQR problem (3) [4]. The optimal RHC then corresponds to the optimal control law for problem (3), which is guaranteed to be recursively feasible and asymptotically stable. However, it is not always possible to choose a large  $N$ , and the optimal RHC will

then correspond to a suboptimal control law for problem (3), which is not guaranteed to be recursively feasible and asymptotically stable. The following conditions specify how to construct the finite-horizon problem so that the optimal RHC still obtains these guarantees.

**Definition 8 (Control Invariant Set)** *A set  $\mathcal{C} \in \mathcal{X}$  is a control invariant set for system (1) subject to constraints (2) if*

$$\mathbf{x}(t) \in \mathcal{C} \implies \exists \mathbf{u}(t) \in \mathcal{U} \text{ such that } \mathbf{A}\mathbf{x}(t) + \mathbf{B}\mathbf{u}(t) \in \mathcal{C}$$

Examples of a control invariant set are  $\mathcal{O}_\infty^{LQR}$ , and the set  $\{\bar{\mathbf{x}}\}$  containing only the equilibrium point.

**Definition 9 (Control Lyapunov Function)** *Suppose the stage cost  $q : \mathbb{R}^{n+m} \rightarrow \mathbb{R}$  is a continuous, positive-definite function. A function  $p : \mathbb{R}^n \rightarrow \mathbb{R}$  that is continuous, positive definite, and satisfies, for every  $\mathbf{x} \in \mathcal{C}$ ,*

$$\min_{\mathbf{u} \in \mathcal{U}, \mathbf{A}\mathbf{x} + \mathbf{B}\mathbf{u} \in \mathcal{C}} (p(\mathbf{A}\mathbf{x} + \mathbf{B}\mathbf{u}) - p(\mathbf{x}) + q(\mathbf{x}, \mathbf{u})) \leq 0,$$

*is called a control Lyapunov function for system (1) over the set  $\mathcal{C}$ .*

The following theorem states that choosing the terminal constraint set  $\mathcal{X}_f$  to be a control invariant set and terminal cost  $p(\mathbf{x})$  to be a control Lyapunov function over  $\mathcal{X}_f$  will guarantee recursive feasibility and asymptotic stability of the RHC  $\mu^*$  corresponding to the optimal planner  $\pi^*$ .

**Theorem 10** *Suppose  $\mathcal{X}, \mathcal{X}_f$ , and  $\mathcal{U}$  contain the origin in their interior and are closed, and in addition that  $\mathcal{X}_f$  is a control invariant set. Suppose the stage cost  $q(\mathbf{x}, \mathbf{u})$  is continuous and positive definite, and choose the terminal cost  $p(\mathbf{x})$  to be a control Lyapunov function over  $\mathcal{X}_f$ . Then, the optimal RHC  $\mu^*$  corresponding to the optimal planner  $\pi^*$  with domain  $\mathcal{X}_0$  is recursively feasible and asymptotically stable with domain of attraction  $\mathcal{X}_0$  for system (1) subject to constraints (2).*

**PROOF.** See [5, Thm 12.1] for recursive feasibility and [5, Thm 12.2] for asymptotic stability.

The choice of cost  $p(\mathbf{x}) = \mathbf{x}_N^T \mathbf{P}_\infty \mathbf{x}_N$  satisfies the conditions of a control Lyapunov function where the stage cost has the form  $q(\mathbf{x}, \mathbf{u}) = \mathbf{x}^T \mathbf{Q}\mathbf{x} + \mathbf{u}^T \mathbf{R}\mathbf{u}$ .

## 6.2 Approximate RHC

Recall that the trained neural network  $\phi(\mathbf{x}|\boldsymbol{\theta})$  represents an approximate planner  $\tilde{\pi}$ , not the optimal planner  $\pi^*$ .

In addition to the conditions stated in Thm. 10, an approximate planner must satisfy two more conditions to guarantee recursive feasibility and asymptotic stability of the corresponding suboptimal RHC.

The condition to guarantee recursive feasibility of the RHC is primal feasibility of the estimated  $\mathbf{z}$  for all feasible initial state parameters  $\mathbf{x} \in \mathcal{X}_0$ . The condition to guarantee asymptotic stability is bounding the suboptimality of the estimated  $\mathbf{z}$  for all feasible initial state parameters  $\mathbf{x} \in \mathcal{X}_0$ . Note that these conditions depend on the specific planner, and not just the construction of the finite-horizon problem (4) from the original infinite-horizon LQR problem (3). These conditions are formally stated in the following theorem.

**Theorem 11** *Suppose  $\mathcal{X}, \mathcal{X}_f$ , and  $\mathcal{U}$  contain the origin in their interior and are closed, and in addition that  $\mathcal{X}_f$  is a control invariant set. Suppose the stage cost  $q(\mathbf{x}, \mathbf{u})$  is a continuous and positive definite function, and choose the terminal cost  $p(\mathbf{x})$  to be a control Lyapunov function over  $\mathcal{X}_f$ . Suppose that an approximate planner  $\tilde{\pi}$  with domain  $\mathcal{X}_0$  is primal feasible, and there exists a function  $\gamma(\mathbf{x})$  where  $\forall \mathbf{x} \in \mathcal{X}_0$ ,*

$$\begin{aligned} 0 &\leq \sigma(\tilde{\pi}(\mathbf{x})|\mathbf{x}) \leq \gamma(\mathbf{x}), \\ \gamma(\mathbf{x}) - q(\mathbf{x}, \mathbf{0}) &\leq 0, \end{aligned} \tag{18}$$

*then the corresponding approximate RHC  $\tilde{\mu}$  is recursively feasible and asymptotically stable with domain of attraction  $\mathcal{X}_0$  for system (1) subject to constraints (2).*

**PROOF.** A similar argument as for the optimal case proves recursive feasibility. See [5, Thm 13.1] for asymptotic stability.

## 6.3 Strategy To Obtain Guarantees

These theorems motivate the following strategy to guarantee recursive feasibility and asymptotic stability of our approximate RHC. We first choose  $\mathcal{X}_f$  to be a control invariant set, and the terminal cost  $p(\mathbf{x})$  to be a control Lyapunov function over  $\mathcal{X}_f$ . We then need to guarantee that our approximate planner  $\tilde{\pi}$  is primal feasible, and the corresponding RHC  $\tilde{\mu}$  will be recursively feasible.

We next set the function  $\gamma(\mathbf{x})$  in Thm. 11 to be the feasible duality gap  $\eta(\mathbf{z}, \boldsymbol{\nu}, \boldsymbol{\lambda}|\mathbf{x})$  in Eqn. (12). We compute  $\eta$  by using primal feasible variables  $\mathbf{z}$  to estimate corresponding dual feasible variables  $\boldsymbol{\nu}, \boldsymbol{\lambda}$ . By Eqn. (12),  $\eta$  will satisfy the first row in Eqn. (18). To satisfy the second row, we need to bound  $\eta$  by the first zero input stage cost  $q(\mathbf{x}, \mathbf{0}) \forall \mathbf{x} \in \mathcal{X}_0$ .

We can thus guarantee recursive feasibility and asymptotic stability of  $\tilde{\mu}$  by obtaining a certificate of primal feasibility and a certificate of suboptimality for  $\tilde{\pi} \forall \mathbf{x} \in \mathcal{X}_0$ .

Sec. 6.4 details our method to determine whether given  $\mathbf{x} \in \mathcal{X}_0$ , the predicted  $\mathbf{z}$  from  $\tilde{\pi}(\mathbf{x})$  satisfies both certificates, and Sec. 7 discusses our strategy in using an on-line primal active set method to ensure that these certificates will be obtained  $\forall \mathbf{x} \in \mathcal{X}_0$ .

#### 6.4 Certificate Evaluation

Evaluating primal feasibility is trivial, since given an initial state parameter  $\mathbf{x}$ , we can check primal feasibility by directly evaluating constraint violation for the predicted  $\mathbf{z}$ . If we obtain a certificate of primal feasibility, the next step is find dual feasible variables  $\boldsymbol{\nu}, \boldsymbol{\lambda}$  that satisfy  $\eta(\mathbf{z}, \boldsymbol{\nu}, \boldsymbol{\lambda} | \mathbf{x}) \leq q(\mathbf{x}, \mathbf{0})$ , which obtains the certificate of suboptimality.

One option is to additionally approximate the dual function [41] with another neural network, but it has a few drawbacks. First, this approach will substantially increase the size of the neural networks, and a smaller network is preferable to reduce inference speed. Second, the optimal dual function is typically not unique. The *linear independence constraint qualification (LICQ)* does not hold when the number of rows in constraint matrices  $\mathbf{G}_{\text{eq}}$  and  $\mathbf{G}_{\text{in}}$  are more than the columns, which is typically the case in most problems. As a result, the Hessian of the concave objective in the dual problem is negative semi-definite [5, Ch. 3.3] and implies that the dual solution may not be unique. This non-uniqueness requires extra care when generating the dual labels and designing the loss function to train a neural network. Finally, separately predicting both the primal and dual variables is redundant, as one can easily be derived from the other.

We use the KKT optimality conditions to derive a set of feasible dual variables from primal variables. For the optimal primal variables  $\mathbf{z}^*$ , this procedure will yield optimal dual variables  $\boldsymbol{\nu}^*, \boldsymbol{\lambda}^*$ . Using the predicted primal variables  $\mathbf{z}$ , the first step is forming a working set  $\mathcal{W}_A$  consisting of the active equality and inequality constraints. Alg. 1 demonstrates how to estimate this working set  $\mathcal{W}_A$  given a set of primal variables  $\mathbf{z}$ . Notice that for any primal feasible  $\mathbf{z}$ ,  $\mathbf{G}_{\text{eq}}\mathbf{z} - \mathbf{E}_{\text{eq}}\mathbf{x} = 0$ , so Alg. 1 assumes that  $\mathcal{W}_A$  will contain all of the equality constraints.

Due to the *complementary slackness* KKT optimality condition, the dual variables corresponding to the inactive constraints should be set to 0. We can thus focus on the dual variables for the remaining active constraints in  $\mathcal{W}_A$ , which sets up the following KKT system:

$$\begin{bmatrix} 2\mathbf{H} & \mathbf{G}_A^T \\ \mathbf{G}_A & \mathbf{0} \end{bmatrix} \begin{bmatrix} \mathbf{z} \\ \boldsymbol{\kappa}_A \end{bmatrix} = \begin{bmatrix} \mathbf{0} \\ \mathbf{w}_A + \mathbf{E}_A\mathbf{x} \end{bmatrix}. \quad (19)$$

The matrices  $\mathbf{G}_A$ ,  $\mathbf{w}_A$ , and  $\mathbf{E}_A$  are constructed using the rows of the active constraints, and  $\boldsymbol{\kappa}_A$  are the dual

---

#### Algorithm 1 Estimate Working Set

---

```

1: procedure WorkingSet( $\mathbf{x}, \tilde{\mathbf{z}}, \delta$ )
2:    $\backslash\backslash$   $\mathbf{x}$  is the initial state parameter
3:    $\backslash\backslash$   $\tilde{\mathbf{z}}$  are the estimated primal variables
4:    $\backslash\backslash$   $\delta \in \mathbb{R}$  is a threshold parameter
5:    $\mathcal{W}_A = \{\}$ 
6:    $\backslash\backslash$  Equality constraints
7:   for  $i = 1 \dots Nn$  do
8:      $\mathcal{W}_A = \mathcal{W}_A \cup i$ 
9:    $\backslash\backslash$  Inequality constraints
10:  for  $i = 1 \dots (Nc_x + c_f + Nc_u)$  do
11:    if  $(\mathbf{G}_{\text{in}}^i \tilde{\mathbf{z}} - \mathbf{w}_{\text{in}}^i - \mathbf{E}_{\text{in}}^i \mathbf{x} \geq -\delta)$  then
12:       $\mathcal{W}_A = \mathcal{W}_A \cup (Nn + i)$ 
13:  return  $\mathcal{W}_A$ 

```

---

variables corresponding to both equality and inequality active constraints. The matrix on the left is called the KKT matrix.

If  $\mathbf{H}$  is positive definite, and if the matrix  $\mathbf{G}_A$  has full row rank, the KKT matrix is invertible. Solving this KKT system yields primal and dual variables that satisfy the *stationarity* KKT condition, expressed in the first row, and *primal feasibility* KKT condition, expressed in the second row.

Given primal feasible  $\mathbf{z}$ , we can construct  $\mathcal{W}_A$ , and thus  $\mathbf{G}_A$ , by using Alg. 1 and ensuring that  $\mathbf{G}_A$  has full row rank. We thus obtain the following equation relating  $\boldsymbol{\kappa}_A$  to  $\mathbf{z}$ :

$$\mathbf{G}_A \mathbf{H}^{-1} \mathbf{G}_A^T \boldsymbol{\kappa}_A = -2\mathbf{G}_A \mathbf{z}. \quad (20)$$

Since  $\mathbf{H}$  is positive definite and  $\mathbf{G}_A$  is full row rank,  $\mathbf{G}_A \mathbf{H}^{-1} \mathbf{G}_A^T$  is positive definite, and thus (20) can be solved for  $\boldsymbol{\kappa}_A$  using Cholesky factorization. It is simple to obtain the dual variables  $\boldsymbol{\nu}, \boldsymbol{\lambda}$  from  $\boldsymbol{\kappa}_A$  based on whether the original dual variable  $\nu^i$  or  $\lambda^i$  is active and set to the corresponding  $\kappa_A^i$ , or inactive and set to 0.

Unless  $\mathcal{W}_A$  corresponds to the active constraints at the optimal solution, the resulting  $\boldsymbol{\kappa}_A$  will be dual infeasible and needs to be corrected. The pair of primal feasible  $\mathbf{z}$  and dual infeasible  $\boldsymbol{\nu}, \boldsymbol{\lambda}$  satisfy the *complementary slackness*, *stationarity*, and *primal feasibility* KKT conditions. If the *dual feasibility* KKT condition were also satisfied, then all the KKT optimality conditions are satisfied and thus  $\mathbf{z}, \boldsymbol{\nu}, \boldsymbol{\lambda}$  must be optimal.

When  $\boldsymbol{\kappa}_A$  is dual infeasible, we can obtain feasible dual variables since the feasible region for the inequality dual variables is the non-negative orthant, and the Euclidean projection is particularly simple because it is the element-wise  $\max(\kappa_A^i, 0)$ . The equality variables are unconstrained. After performing the projection, Eqn. (19) will no longer be satisfied, as we have swapped satisfying the *stationarity* condition with the *dual feasibility* KKT condition.

Given a primal feasible  $\mathbf{z}$ , this procedure will always



yield dual feasible  $\nu, \lambda$ . We can then check if the feasible duality gap  $\eta(\mathbf{z}, \nu, \lambda | \mathbf{x}) < q(\mathbf{x}, \mathbf{0})$ , which implies that  $\sigma(\mathbf{z} | \mathbf{x}) < q(\mathbf{x}, \mathbf{0})$ , and thus satisfies the second row in the conditions for Eqn. (18). Successfully finding these dual feasible variables obtains a certificate of suboptimality.

The above procedure only checks whether the certificates of primal feasibility and suboptimality are satisfied, but does not guarantee satisfaction. The predicted primal variables  $\mathbf{z}$  may not necessarily be primal feasible and will not yield the certificate of primal feasibility. In addition, the procedure may not yield the certificate of suboptimality because the predicted primal variables or derived dual feasible variables are too conservative, and the resulting  $\eta > q(\mathbf{x}, \mathbf{0})$ . The following Sec. 7 details how we guarantee satisfying both certificates  $\forall \mathbf{x} \in \mathcal{X}_0$  by using an online primal active set method, and thus obtain the guarantees on recursive feasibility and asymptotic stability of the approximate RHC  $\tilde{\mu}$ .

## 7 Obtaining Guarantees with Online Primal Active Set Solver

For a planner  $\pi$  represented solely by an offline trained neural network  $\phi$ , it is a challenging to guarantee that both certificates of primal feasibility and suboptimality are satisfied for all states  $\mathbf{x} \in \mathcal{X}_0$ . Most guarantees that can be provided on neural networks will be statistical [16], as there will be a chance that the neural network outputs an extremely poor prediction.

Our approach is to instead use an online method to ensure satisfaction of these conditions for all states  $\mathbf{x} \in \mathcal{X}_0$ . We utilize a primal active set solver [39, Ch. 16] because it is distinguished among QP solver techniques in that it can be accelerated through warm starts from good initializations from the neural network, and it can also be terminated early once the certificates of primal feasibility and suboptimality are achieved. Methods such as interior-point methods are difficult to warm start [18], and other non-primal active set methods do not guarantee primal feasibility of intermediate iterates and cannot be terminated early [10]. Intuitively, the neural network removes the early iterations of the solver, and checking the criteria of Thm. 11 removes the final iterations.

### 7.1 Warm Starting and Early Termination

Active set methods solve inequality-constrained QPs by solving a sequence of equality-constrained quadratic subproblems [39]. These solvers are closely related to the concept of working sets introduced in Sec. 6, as they explicitly maintain and update  $\mathcal{W}_A$ , where each intermediate working set represents an equality-constrained quadratic subproblem. The goal of these procedures is to determine the optimal working set  $\mathcal{W}_A^*$ , after which solving the corresponding KKT system (19) will yield the optimal primal  $\mathbf{z}^*$  and dual  $\nu^*, \lambda^*$  variables.

---

### Algorithm 2 Explicit-Implicit Planner

---

```

1: procedure ObtainCertificate( $\tilde{\mathbf{z}}, \mathbf{x}, \mathcal{A}$ )
2:    $\backslash\backslash$   $\mathbf{x}$  is the initial state parameter
3:    $\backslash\backslash$   $\tilde{\mathbf{z}}$  is the initial neural network prediction
4:    $\backslash\backslash$   $\mathcal{A}$  is the primal active set solver
5:   Obtain certificate of primal feasibility and
6:   suboptimality according to Sec. 6.4.
7:   if both certificates obtained then
8:     return  $\tilde{\mathbf{z}}$ 
9:   else
10:    Warm Start  $\mathcal{A}$  with  $\tilde{\mathbf{z}}$  according to Sec. 7.1.
11:    Perform Phase I of  $\mathcal{A}$  and obtain certificate of
12:    primal feasibility
13:    while no certificate of suboptimality do
14:      Update  $\tilde{\mathbf{z}}$  via Phase II iteration of  $\mathcal{A}$ .
15:      Attempt to obtain certificate of suboptimality
16:      according to Sec. 6.4.
17:    return  $\tilde{\mathbf{z}}$ 

```

---

The general approach is to start with some initial guess of the active set  $\mathcal{W}_A^0$ , and proceed by adding and removing constraints from this set until  $\mathcal{W}_A^*$  is found. During the course of solving the QP, these active set algorithms maintain intermediate terms such as primal variables, dual variables, basis variables, and factorizations of the basis and Hessian, with the specific terms tracked being dependent on the particular solver chosen. Combined these intermediate terms constitute the *solver state*.

Active set methods are well-suited to acceleration due to good initialization [39]. This strategy is called a warm start if part of the solver state is initialized, or a hot start if all of the solver state is initialized. Using Alg. 1 in Sec. 6 on the neural network primal prediction  $\mathbf{z}$  can yield a working set to initialize  $\mathcal{W}_A^0$ .

We reduce online computation by terminating the online solver once the criteria in Thm. 11 are satisfied. Primal active set solvers explicitly find and maintain primal feasibility of intermediate iterates, which is necessary to satisfy the certificate of primal feasibility prior to reaching optimality. These solvers are split into two phases. In *Phase I*, the solver first finds an initial primal feasible point by solving a linear feasibility program. Starting from this primal feasible point, *Phase II* updates the primal solution and the working active set while maintaining primal feasibility. As a result, once *Phase I* completes, we will obtain a certificate of primal feasibility. During *Phase II*, we check the duality gap at the intermediate iterates using the techniques described in Sec. 6 in order to obtain the certificate of suboptimality.

### 7.2 Suboptimal Planner with Guarantees

Using these ideas, we reach our final hybrid explicit-implicit algorithm that computes another approximate planner  $\hat{\pi}$  by following the procedure in Alg. 2. This procedure is guaranteed to terminate in finite time as the

---

**Algorithm 3** Line Solve Algorithm

---

```

1: procedure LineSolve( $s_0, \mathbf{x}_g, d$ )
2:    $\backslash\backslash$   $s_0 = (\mathbf{x}_s, \mathbf{z}_s, \boldsymbol{\nu}_s, \boldsymbol{\lambda}_s, \mathbf{q}_s)$  is a seed tuple of state,
   optimal primal variables, dual variables, and auxiliary
   solver state variables.
3:    $\backslash\backslash$   $\mathbf{x}_g$  is a goal state
4:    $\backslash\backslash$   $d$  is the step size
5:    $\mathbf{x}_n = \frac{\mathbf{x}_g - \mathbf{x}_s}{\|\mathbf{x}_g - \mathbf{x}_s\|}$ 
6:    $N_{iterations} = \text{ceil}(\frac{\|\mathbf{x}_g - \mathbf{x}_s\|}{d})$ 
7:   for  $i = 1 \dots N_{iterations}$  do
8:      $\mathbf{x}_i = \mathbf{x}_s + i(d\mathbf{x}_n)$ 
9:     (success,  $s_i$ ) = HotStart( $s_{i-1}$ )
10:    if success then
11:       $\mathcal{D} = \mathcal{D}.\text{append}(s_i)$ 
12:    else
13:      return  $\mathcal{D}$ 
14: return  $\mathcal{D}$ 

```

---

active set method will reach the optimal solution in finite time [39, Ch. 16]. In addition, for all  $\mathbf{x} \in \mathcal{X}_0$ ,  $\hat{\pi}$  will also obtain certificates of primal feasibility and suboptimality. Finally, given that the terminal constraint and terminal cost were chosen to satisfy the conditions specified in Thm. 11, the resulting  $\hat{\mu}$  is guaranteed to be recursively feasible and asymptotically stable according to Thm. 11.

## 8 Scaling to Large Systems

The motivation for using a neural network is scaling to large systems and long time horizons. While the previous sections detailed our approach to compute an approximate planner with guarantees on the corresponding RHC, this section discusses the particular challenges of function approximation in large MPC problems which arise during the training data set generation process. Our approach to overcome these challenges draws on ideas from *geometric random walks* [35] and *quasi Monte Carlo (QMC) sequences* [28, 32].

The domain of the planner  $\pi$  is the polyhedron  $\mathcal{X}_0$ . The main challenge is that, as previously mentioned in Sec. 3.2, computing an explicit (halfspace or vertex) representation of  $\mathcal{X}_0$  is computationally intractable for large systems. Instead,  $\mathcal{X}_0$  is defined by a membership oracle [35] which on an input  $\mathbf{x} \in \mathbb{R}^n$  returns Yes if  $\mathbf{x} \in \mathcal{X}_0$ , and No otherwise. In mp-QP problems, this membership oracle is a QP solver that given a parameter  $\mathbf{x}$  solves the corresponding QP (5).

We will generate a training data set to train the neural network by sampling data points  $\mathbf{x}$  from the domain  $\mathcal{X}_0$ . As a result, we need a method that can sample data points from a convex set defined by a membership oracle which will also scale to high dimensions. One method is *rejection sampling*, which involves sampling from a superset of  $\mathcal{X}_0$  and querying the membership oracle for

---

**Algorithm 4** Data Set Generation Algorithm

---

```

1: procedure GenData( $\mathcal{G}, \mathcal{S}, N, d$ )
2:   Initialize  $\mathcal{D} = \emptyset$ 
3:   for  $i = 1 \dots N$  do
4:     Choose  $\mathbf{x}_g$  the  $i^{\text{th}}$  element of  $\mathcal{G}$ 
5:     Sample seed tuple  $s_0 \in \mathcal{S}$ 
6:      $\mathcal{D}_i = \text{LineSolve}(s_0, \mathbf{x}_g, d)$ 
7:      $\mathcal{D} = \mathcal{D} \cup \mathcal{D}_i$ 
8:     Place last tuple of  $\mathcal{D}_i$  in  $\mathcal{S}$ 
9:   return  $\mathcal{S}, \mathcal{D}$ 
10:
11: procedure
12:   DataWrapper( $N_{trn}, N_{bf}, N_{tst}, d, \mathcal{X}$ )
13:    $\backslash\backslash$   $N_{trn}$  is number of goal points for the train set
14:    $\backslash\backslash$   $N_{bf}$  is number of goal points for the buffer set
15:    $\backslash\backslash$   $N_{tst}$  is number of goal points for the test set
16:    $\backslash\backslash$   $d$  is the step size
17:    $\backslash\backslash$   $\mathcal{X}$  is the sampling hypercube
18:   Set the sequence  $[\mathcal{G}_{trn}, \mathcal{G}_{bf}, \mathcal{G}_{tst}]$  to be the first
19:    $N_{trn} + N_{bf} + N_{tst}$  points of Sobol sequence in
20:    $[0, 1]^n$  rescaled to  $\mathcal{X}$ 
21:   Initialize seed set  $\mathcal{S}_0 = \{(\mathbf{x}_0, \mathbf{z}_0, \boldsymbol{\nu}_0, \boldsymbol{\lambda}_0, \mathbf{q}_0)\}$ 
22:    $\backslash\backslash$  Train, Buffer, Test
23:    $\mathcal{S}_{trn}, \mathcal{D}_{trn} = \text{GenData}(\mathcal{G}_{trn}, \mathcal{S}_0, N_{trn}, d)$ 
24:    $\mathcal{S}_{bf}, \mathcal{D}_{bf} = \text{GenData}(\mathcal{G}_{bf}, \mathcal{S}_{trn}, N_{bf}, d)$ 
25:    $\mathcal{S}_{tst}, \mathcal{D}_{tst} = \text{GenData}(\mathcal{G}_{tst}, \mathcal{S}_{bf} \setminus \mathcal{S}_{trn}, N_{tst}, d)$ 
26:   return  $\mathcal{D}_{trn}, \mathcal{D}_{tst}$ 

```

---

each point. A point is added to the data set  $\mathcal{D}$  only if the oracle returns Yes. An example of a sampling superset is  $\mathcal{X}$ , as  $\mathcal{X}_0 \subseteq \mathcal{X}$ .

Unfortunately, rejection sampling will not scale to high dimensions. First, the cost of querying the membership oracle becomes more expensive with higher dimensions, as the corresponding QP (5) becomes larger. More prohibitively, the probability of sampling a feasible state will, in general, become very small, which we empirically observe in the MPC application (see Fig. 8 in Sec. 9). This phenomenon can be understood by comparing  $\text{Vol}(\mathcal{X}_0)$ , the volume of  $\mathcal{X}_0$ , with  $\text{Vol}(\mathcal{X})$  (or more generally to a sampling superset) as the time horizon, states, and inputs increase. With an increasing time horizon  $N$ ,  $\mathcal{X}_0$  will shrink [5, Rmk. 11.4] until  $\mathcal{X}_0$  becomes the maximal stabilizable set for control invariant set  $\mathcal{X}_f$  [5, Rmk. 11.3], and there is no guarantee that  $\mathcal{X}_0$  will become the maximal stabilizable set in finite time [5, Sec. 10.2]. This shrinking occurs since there will be more constraints in QP (5) with increasing  $N$ . As a result,  $\frac{\text{Vol}(\mathcal{X}_0)}{\text{Vol}(\mathcal{X})}$  will typically decrease with increasing  $N$  and the probability of a sampled point from  $\mathcal{X}$  lying in  $\mathcal{X}_0$  will likewise decrease for typical distributions such as the uniform distribution over the convex set.

We can intuitively understand how  $\frac{\text{Vol}(\mathcal{X}_0)}{\text{Vol}(\mathcal{X})}$  behaves with increasing states and inputs by recalling the classic *curse of dimensionality* example  $\lim_{n \rightarrow \infty} \frac{\text{Vol}(\mathcal{B}_n)}{\text{Vol}(\mathcal{C}_n)} = 0$ , where

$\mathcal{B}_n$  is an n-dimensional hypersphere of diameter 2 and  $\mathcal{C}_n$  is an n-dimensional hypercube with side length 2 that is the minimum bounding hypercube for  $\mathcal{B}_n$ . With increasing dimensions, most of the volume in a cube is contained in the corners. A similar phenomenon is likely to occur in the MPC application as the set difference  $\mathcal{X} \setminus \mathcal{X}_0$  will contain initial states closer to the edges and corners of  $\mathcal{X}$  rather than the origin.

To surmount this problem, we develop an algorithm motivated by *geometric random walks* [35], which sample from convex sets using the membership oracle. To sample from a given distribution, these methods set up a random walk whose steady state is the desired distribution to sample from. Examples of these random walks are the *grid walk* which starts from the interior of the convex set and moves to neighboring points on a grid, or the *hit and run walk* which picks a random line  $l$  at the current point  $\mathbf{x}$  and goes to a random point on the chord  $l \cap \mathcal{X}_0$ . At each potential point  $\mathbf{x}'$ , the random walk will query the membership oracle and move to  $\mathbf{x}'$  if the oracle returns Yes, otherwise stay at the current point  $\mathbf{x}$ .

The states reached by this random walk will lie inside the convex set and overcome the previous sampling challenges. Since the desired distribution to sample is the stationary distribution, effective sampling with these methods requires the distribution of the current point to converge rapidly to its steady state, which is called *mixing*. Many of the technical details are beyond the scope of this manuscript and are described in [35], but a key positive result in this theory is that for convex sets and distributions with logconcave density (which include most of the common distributions such as the uniform distribution over a convex set), various geometric random walk strategies will mix in time polynomial to the dimension of the problem. As a result, these techniques can generate samples efficiently even in high dimensions.

The geometric random walk is an example of a Monte Carlo method which randomly samples points to include in the data set. *QMC* methods instead generate a deterministic low-discrepancy sequence of points that are “well distributed” compared to random sampling in the sense that the generated points are spread apart [24, 28]. These techniques are widely used in mathematical finance to evaluate high-dimensional integrals. In addition, the concept of low-discrepancy data sets has recently been explored in Analytical Learning Theory to provide bounds on generalization [20]. One example of a *QMC* low-discrepancy sequence is the Sobol sequence [32], and there are efficient algorithms to construct these sequences [2].

### 8.1 Data Set Generation Algorithm

Our proposed data set generation algorithm merges ideas from both geometric random walks and QMC se-

quences. The full algorithm is described in Algs. 3 and 4, and Figs. 1a and 1b provide illustrations of its behavior on Sys. 1. While our proposed algorithm does not satisfy the criteria of a geometric random walk, it takes advantage of attractive behaviors from both theories, and empirically performs well on large systems.

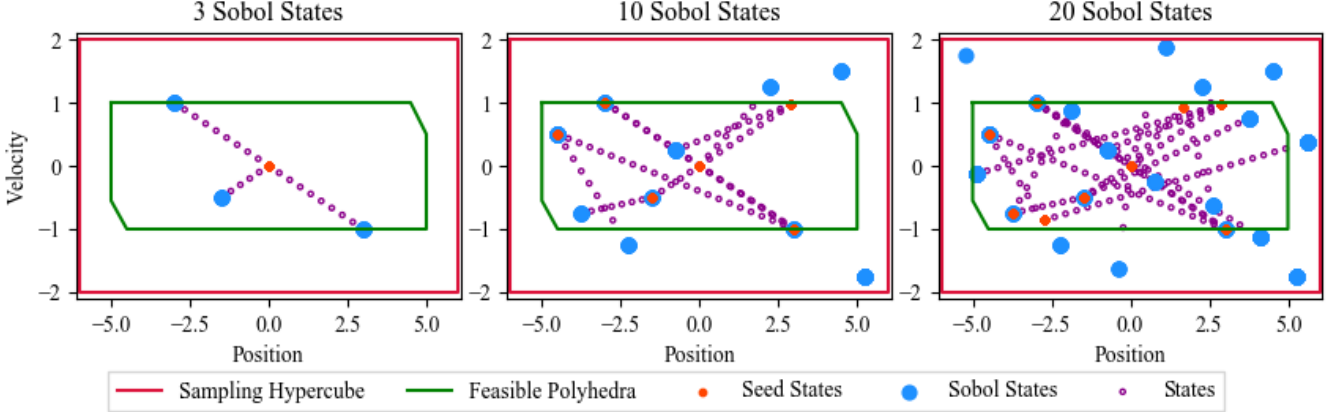
Our algorithm initializes and updates a set of seed states that are known to be in  $\mathcal{X}_0$ . It is also given a set of goal states that correspond to the Sobol sequence. See Fig. 1a for an illustration of the first few points of the Sobol sequence in 2 dimensions. The algorithm proceeds by randomly selecting a seed state and pairing it with the next goal state in the Sobol sequence. It then performs the line solve subprocedure detailed in Alg. 3. The subprocedure queries the membership oracle (QP solver) along the line segment formed by the seed and goal state starting at the seed state, where the oracle returns the corresponding optimal primal and dual variables for states determined to be in  $\mathcal{X}_0$ .

If the membership oracle returns No during this process, the subprocedure terminates, as all remaining points in the line segment will lie outside of  $\mathcal{X}_0$  due to the convexity of  $\mathcal{X}_0$ . Otherwise the subprocedure terminates once it reaches the goal state. Upon termination in either case, the subprocedure returns the set of intermediate states that were determined to be feasible, as well as the corresponding optimal primal and dual variables.

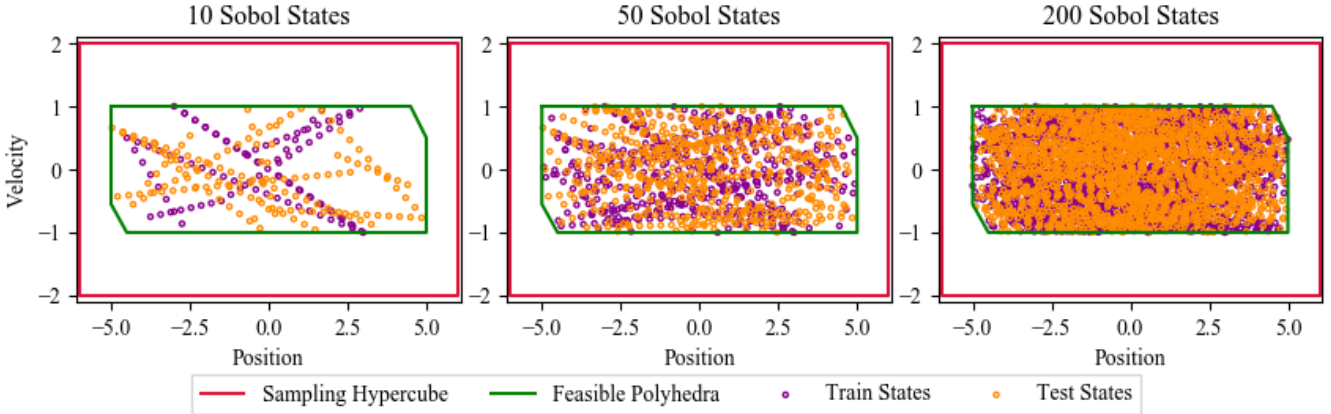
Our algorithm receives this set of feasible intermediate states, and includes it into the aggregated data set. In addition, it updates the set of seed states with the last state that the subprocedure determined to be in  $\mathcal{X}_0$ . The intuition for using the last intermediate state is to spread out the states in the seed set. While geometric random walks typically are not initialized from a pre-determined starting point [35], we initialize our seed set  $\mathcal{S}_0$  with the equilibrium state, known to be inside  $\mathcal{X}_0$ , and its corresponding optimal solver state.

Our proposed algorithm is thus similar to the hit and run random walk method with a few differences. The hit and run random walk has a subprocedure similar to our line solve subprocedure. It starts from the current state, which corresponds to our seed state, and randomly chooses a line segment  $l$ , which can be implemented by randomly choosing a goal state. On the other hand, our algorithm randomly chooses the seed state from a set of states that are updated throughout the algorithm, and deterministically chooses a goal state from a Sobol sequence that has been constructed to be spread apart. We made this modification to introduce the Sobol sequence and take advantage of its ability to generate goal points that are spread apart.

In addition, the subprocedure in hit and run only returns 1 state randomly selected on the line segment, whereas our line solve subprocedure performs a search along this



(a) **Space Filling Generator:** Illustration of the data generation procedure with varying number of goal (Sobol) states.



(b) **Train and Test Distribution** Illustration of the different distributions for the train and test set. With enough goal (Sobol) states, both fill the entire feasible polyhedra.

Fig. 1. Proposed efficient data set generation algorithm for the double integrator system (2 state dimensions).

line segment and returns all the intermediate states determined to be feasible. By performing this line search, we can more efficiently query our membership oracle by solving a sequence of closely related points using hot starts described in Sec. 7.1. This behavior of moving to a successor state that is in close proximity to the current state is found in the grid walk, but not the hit and run walk, and solving for intermediate states on the line segment reintroduces this behavior.

Neural networks are typically trained on a train set, and evaluated on a test set. Ideally, the samples are *i.i.d.*, and as a result the test set is completely independent of the train set, but drawn from the same underlying distribution. As a result, performance on the test set is a good indicator of expected performance on the underlying distribution. While geometric random walks provide a way to sample nearly independent points [35, Thm. 7.3], our proposed algorithm does not satisfy the criteria of a geometric random walk. As a result, we take extra care when creating the train and test data set split, and the procedure is detailed in Alg. 4.

We introduce a buffer set the purpose of which is to generate additional seed states that do not appear in the train data set. The Sobol points are divided into three segments, denoted as train, buffer, and test. We first create the train data set by iterating through each of the train Sobol points and updating the train seed set. We then copy the train seed states generated from this process to form the buffer seed set, and iterate through the buffer Sobol points while updating the buffer seed set. After we exhaust the buffer Sobol points, we form the test seed set by taking the set difference between the buffer seed set and the train seed set. As a result, all of these seed points in the test seed set do not appear in the train data set, and the test Sobol points will also not appear in the train set. Using these test seed states and test goal states, we can then generate the test set. The illustration of the different trajectories generated in the train and test sets are depicted in Fig. 1b.

System		Train size thousands	Buffer size thousands	Test size thousands	Data Gen. time total	Train time total	Test time per example
Sys. 1	Total (Sobol)	15 (2)	4 (0.4)	4 (0.4)	1.5 s	100 s	1.0 ms
Sys. 2	Total (Sobol)	863 (200)	173 (40)	173 (40)	3.0 m	1.4 h	3.1 ms
Sys. 3	Total (Sobol)	174 (20)	35 (4)	35 (4)	1.0 m	0.4 h	3.3 ms
Sys. 4	Total (Sobol)	1,754 (400)	175 (40)	175 (40)	5.2 h	20 h	38.8 ms

Fig. 2. Overview of the data set sizes and time statistics.

## 9 Numerical Examples

We provide numerical examples of our approach on four systems. The purpose of these examples is to demonstrate that our proposed approach has the ability to scale to large problems, as well as highlight the challenges that arise when scaling to a high dimensional system. We use Tensorflow [1] to train and evaluate the neural networks, SQOPT [11] as our primal active set solver, and MPT3 [14] to compute the terminal cost and constraints. Fig. 2 provides an overview of the data sets for each system we evaluated our approach on. These results were generated using dual Xeon E5-2683 v4 CPUs with 32 cores for the data set generation, and two NVIDIA Titan X Pascal GPUs for the training.

### 9.1 System Descriptions

The first system we evaluated is the double integrator defined in Sys. 1. It is a second-order system that models the dynamics of a mass in 1-D space under a force input.

**System 2 (Quadrotor)** *The differential flatness of quadrotor systems allows us to generate trajectories in the space of flat outputs (position, yaw and their derivatives) that can be followed by the underactuated quadrotor [25, 26]. We can apply MPC for quadrotor trajectory generation by considering the time-invariant continuous-time system:*

$$\dot{\mathbf{x}} = \mathbf{A}_c \mathbf{x} + \mathbf{B}_c \mathbf{u},$$

where

$$\mathbf{A}_c = \begin{bmatrix} 0 & \mathbf{I}_3 & 0 & 0 \\ 0 & 0 & \mathbf{I}_3 & 0 \\ 0 & 0 & 0 & \mathbf{I}_3 \\ 0 & 0 & 0 & 0 \end{bmatrix}, \quad \mathbf{B}_c = \begin{bmatrix} 0 \\ 0 \\ 0 \\ \mathbf{I}_3 \end{bmatrix}.$$

There are  $n = 12$  states and  $m = 3$  inputs. The  $3 \times 3$  sub-matrices correspond to position, velocity, accelera-

System	Layer Widths	Num. Parameters
Sys. 1	<b>2</b> , 32, 32, <b>30</b>	2,142
Sys. 2	<b>12</b> , 32, 32, <b>300</b>	89,900
Sys. 3	<b>12</b> , 32, 64, 128, 256, <b>450</b>	159,522
Sys. 4	<b>36</b> , 128, 128, 256, 256, 512, 512, <b>2250</b>	1,668,554

Fig. 3. Neural network architectures. Each layer is fully connected and followed by the ReLu nonlinearity. Bolded are the input and output sizes of the network.

tion, and jerk. We discretize this continuous time system using Euler discretization with a time step of 0.1. The constraints are given by  $\mathbf{A}_x = [\mathbf{I}_{12}, -\mathbf{I}_{12}]^T$ ,  $\mathbf{b}_x = [10 \cdot \mathbf{1}_3, 5 \cdot \mathbf{1}_3, 3 \cdot \mathbf{1}_3, 1 \cdot \mathbf{1}_3, 10 \cdot \mathbf{1}_3, 5 \cdot \mathbf{1}_3, 3 \cdot \mathbf{1}_3, 1 \cdot \mathbf{1}_3]^T$ , and input constraints  $\mathbf{A}_u = [\mathbf{I}_3, -\mathbf{I}_3]^T$ ,  $\mathbf{b}_u = [\mathbf{1}_3, \mathbf{1}_3]^T$ . The cost matrices are  $\mathbf{Q} = \mathbf{I}_{12}$  and  $\mathbf{R} = \mathbf{I}_3$ . For the receding horizon controller, we choose a time horizon  $N = 20$ , the terminal region  $\mathcal{X}_f$  to be  $\mathcal{O}_\infty^{LQR}$ , and the terminal cost  $\mathbf{x}_N^T \mathbf{P}_\infty \mathbf{x}_N$ . The number of constraints are  $c_x = 24$ ,  $c_f = 246$ , and  $c_u = 6$ . The primal variables have dimension 300, the dual variables corresponding to the inequality constraints have dimension 732, and the dual variables corresponding to the equality constraints have dimension 240.

**System 3 (Oscillating Masses)** *The oscillating masses system, introduced in [37], is a linear system that can be easily scaled to large dimensions by increasing the number of masses and springs in the system. We use 6 masses with a mass of 1, and 3 springs with a spring constant  $c = 1$  and damping constant  $d = 0.1$ . Let  $a = -2c$  and  $b = -2$ . The system is defined as*

$$\dot{\mathbf{x}} = \mathbf{A}_c \mathbf{x} + \mathbf{B}_c \mathbf{u},$$

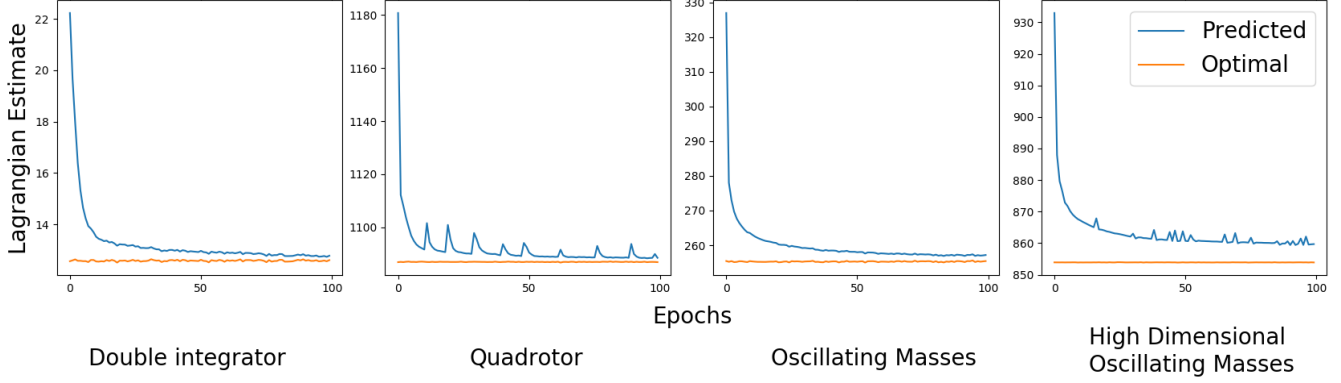


Fig. 4. Training metrics: The Lagrangian Loss is defined in Eqn. (17), and the Lagrangian Estimate is defined in Eqn. (9).

where

$$\mathbf{A}_c = \begin{bmatrix} 0 & \dots & 0 & \dots & 0 & 1 & \dots & 0 & \dots & 0 \\ \vdots & \ddots & & \ddots & \vdots & \vdots & \ddots & & \ddots & \vdots \\ 0 & & 0 & & 0 & 0 & & 1 & & 0 \\ \vdots & \ddots & & 0 & \dots & \vdots & \ddots & & 0 & 1 & 0 \\ 0 & \dots & 0 & & 0 & 0 & \dots & 0 & 0 & 0 & 1 \\ \hline a & c & 0 & \dots & 0 & b & d & 0 & \dots & 0 \\ c & a & c & \ddots & \vdots & d & b & d & \ddots & \vdots \\ 0 & \ddots & \ddots & \ddots & \vdots & 0 & 0 & \ddots & \ddots & \ddots & 0 \\ \vdots & \ddots & c & a & c & \vdots & \ddots & d & b & d \\ 0 & \dots & 0 & c & a & 0 & \dots & 0 & d & b \end{bmatrix}, \quad (21)$$

$$\mathbf{F} = \begin{bmatrix} 1 & 0 & 0 \\ -1 & 0 & 0 \\ 0 & 1 & 0 \\ 0 & 0 & 1 \\ 0 & -1 & 0 \\ 0 & 0 & 1 \end{bmatrix}, \quad \mathbf{B}_c = \begin{bmatrix} \mathbf{0} \\ \mathbf{F} \end{bmatrix}, \quad (22)$$

There are  $n = 12$  states, and  $m = 3$  inputs. We discretize this system using a first-order hold model and time step of 0.5. The cost terms are  $\mathbf{Q} = \mathbf{I}_{12}$ ,  $\mathbf{R} = \mathbf{I}_3$ , subject to state constraints  $\mathbf{A}_x = [\mathbf{I}, -\mathbf{I}]^T$ ,  $\mathbf{b}_x = 4 \cdot \mathbf{1}$ , and input constraint  $\mathbf{A}_u = [\mathbf{I}, -\mathbf{I}]^T$ ,  $\mathbf{b}_u = 0.5 \cdot \mathbf{1}$ . For the receding horizon controller, we choose a time horizon  $N = 30$ , the terminal region  $\mathcal{X}_f$  to be  $\mathcal{O}_\infty^{LQR}$ , and the terminal cost  $\mathbf{x}_N^T \mathbf{P}_\infty \mathbf{x}_N$ . The constraint sizes are  $c_x = 24$ ,  $c_f = 104$ , and  $c_u = 6$ . The primal variables have dimension 450, the dual variables corresponding to the inequality constraints have dimension 1004, and the dual variables corresponding to the equality constraints have dimension

360.

#### System 4 (High Dimensional Oscillating Masses)

The high dimensional oscillating masses system is the largest system that we consider. It is a scaled up version of the original oscillating masses system with  $n = 36$  states and  $m = 9$  inputs. The system matrix  $\mathbf{A}_c$  has 36 dimensions defined in Eqn. (21). The input matrix is  $\mathbf{B}_c = [\mathbf{0} \mid \mathbf{I}_3 \otimes \mathbf{F}^T]^T$ . The cost and constraint terms are chosen similarly as in the oscillating masses system.

For the receding horizon controller, we choose a time horizon  $N = 50$ , the terminal region  $\mathcal{X}_f$  to be  $\mathcal{O}_\infty^{LQR}$ , and the terminal cost  $\mathbf{x}_N^T \mathbf{P}_\infty \mathbf{x}_N$ . The constraint sizes are  $c_x = 72$ ,  $c_f = 408$ , and  $c_u = 18$ . The primal variables have dimension 2250, the dual variables corresponding to the inequality constraints have dimension 4908, and the dual variables corresponding to the equality constraints have dimension 1800.

#### 9.2 Training Statistics

We trained our neural networks with the Lagrangian loss function described in Eqn. (17). The neural networks are trained with the Adam optimizer [21] for 100 epochs. The network architectures and training parameters are listed in Fig. 3. The network depths were chosen using Eqn. (14), and the widths were chosen by trial and error. Each hidden layer of the neural networks are followed by the ReLu activation function. We take 2.5 – 10% (depending on the system) samples from the training set as a held-out validation set. The validation set is only used to evaluate the training loss to avoid over-fitting or under-fitting and is not used to update the neural network weights.

Graphs of the training metrics are displayed in Fig. 4, which compares the Lagrangian defined in Eqn. (9) for the predicted versus optimal primal variables over the course of training. The estimated Lagrangian uses the neural network predicted primal variables and the optimal dual variables, while the optimal Lagrangian uses

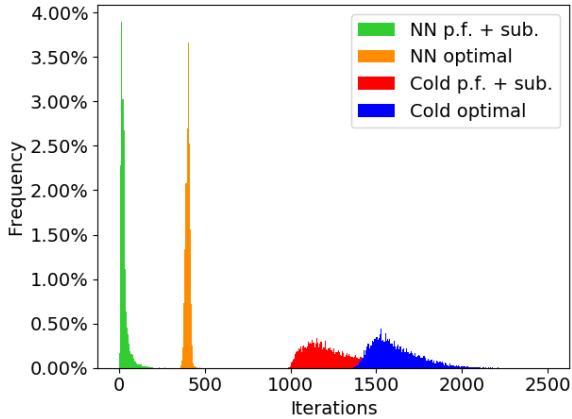


Fig. 5. (Sys. 4) Histogram of iterations for both NN and cold start initialization methods and *p.f. + sub.* and *optimal* termination methods.

the optimal primal and dual variables. Given the optimal dual variables, the optimal primal variables minimize the corresponding Lagrangian. As a result, the optimal Lagrangian is a lower bound to the estimated Lagrangian. The least squares Lagrangian loss in Eqn. (17) attempts to minimize the square of the gap between the two curves. This gap is a proxy metric for the suboptimality level as described in Sec. 5.

### 9.3 Test Metrics

We compare our method in Fig. 7 to the baseline of initializing the active set method using a cold start and solving to the optimal solution on the test set. Our goal is to quantify the impact of both initializing the solver with the neural network, and terminating the solver early according to the early termination criteria. The two main metrics we report are the number of iterations executed, both as an absolute number and as a percentage of the baseline method, and the suboptimality level as a percentage of the baseline method. For each system and initialization method, we report these metrics after the primal feasibility condition has been met (*p.f.*), the primal feasibility and suboptimality criteria has been met (*p.f. + sub.*), and when optimality has been met. Our approach uses a neural network initialization and termination upon satisfaction of the primal feasibility and suboptimality criteria (NN *p.f. + sub.*).

Our method reduces the number of active set iterations significantly, especially for higher dimensional systems such as Sys. 4. Fig. 5 displays a histogram of the number of iterations for our method compared to the baseline methods for Sys. 4 on the test set. For this system, the neural network initialization reduces the number of iterations by  $\sim 1230$  iterations based on the difference between NN *p.f. + sub.* compared to Cold *p.f. + sub.* The early termination according to the criteria reduces the number of iterations by  $\sim 379$ , which can be measured

Sys. 4	Average Time (ms)		
Method	Neural Network	Active Set Solver	Total
Cold <i>optimal</i>	—	336	336
Hot <i>optimal</i>	—	74	74
NN <i>p.f. + sub.</i> (Ours)	<b>0.8</b>	<b>38</b>	<b>39</b>

Fig. 6. (Sys. 4) Average time required to solve high dimensional oscillating masses using cold start in testing, our method in testing, and hot start in data generation

by taking the difference between NN *optimal* compared to NN *p.f. + sub.*, or between Cold *optimal* and Cold *p.f. + sub.* Overall, our method reduces significantly the number of iteration to 1.7% of that using the baseline method. Fig. 7 also highlights the number of iterations required to first reach the primal feasibility condition, and then the suboptimality condition. For most of the high dimensional systems, the extra effort required to reach the suboptimality criteria is minimal.

The effect of the reduced number of iterations on actual inference times for Sys. 4 is highlighted in Fig. 6, which reports inference time of our method compared to the baseline of a Cold *optimal*. We also compare it to the Hot *optimal* method we use to generate the data set. Note that applying this Hot start method requires solving a sequence of closely related problems, whereas our method is not limited to those scenarios.

Using our method, we are able to achieve an order of magnitude increase in speed compared to the baseline method, and a two-fold increase compared to the Hot start method. In addition, the bulk of the time is spent on the active set iterations, as the inference time for the neural network is only 0.8 ms, emphasizing the benefit of using the neural network to accelerate the active set solver. The one order of magnitude speedup is obtained with SQOPT, which incurs unnecessary costs in terminating the solver to check the termination criteria externally. Based on the improvement in the number of iterations, we believe that a dedicated solver which is able to easily perform the termination criteria checks can achieve an even greater speedup.

In addition to measuring the number of iterations, Fig. 7 also measures the quality of each method according to the suboptimality level compared to the baseline method. For the high dimensional systems, when initializing with the neural network, the suboptimality level is low even when only the primal feasibility condition is satisfied. This is in contrast to the cold start methods, where only achieving primal feasibility results in a high suboptimality level, and the suboptimality crite-

System	Initialization Method	Termination Criteria	Iterations ( <i>Absolute</i> )	Iterations ( <i>% of Cold opt.</i> )	Suboptimality ( <i>% of Cold opt.</i> )
Sys. 1	Neural Network	p.f.	$1.0 \pm 0.1$	$8.9 \pm 1.0$	$1400.0 \pm 3867.0$
		<b>p.f. + sub.</b>	<b><math>7.2 \pm 4.9</math></b>	<b><math>64.2 \pm 44.0</math></b>	<b><math>12.0 \pm 96.3</math></b>
Sys. 1	Cold	optimal	$12.2 \pm 3.3$	$109 \pm 31.5$	—
		p.f.	$1.1 \pm 0.3$	$9.7 \pm 2.4$	$200.7 \pm 121.4$
Sys. 1	Cold	p.f. + sub.	$9.5 \pm 3.8$	$83.5 \pm 34.0$	$14.3 \pm 34.0$
		optimal	<b><math>11.5 \pm 1.9</math></b>	—	—
Sys. 2	Neural Network	p.f.	$8.2 \pm 5.15$	$8.3 \pm 5.1$	$1.2 \pm 1.0$
		<b>p.f. + sub.</b>	<b><math>17.8 \pm 10.4</math></b>	<b><math>17.8 \pm 10.2</math></b>	<b><math>0.3 \pm 0.4</math></b>
Sys. 2	Cold	optimal	$57.9 \pm 7.6$	$59.0 \pm 9.3$	—
		p.f.	$32.5 \pm 10.7$	$32.6 \pm 9.7$	$19.7 \pm 12.6$
Sys. 2	Cold	p.f. + sub.	$62.1 \pm 15.5$	$62.5 \pm 13.3$	$0.8 \pm 0.8$
		optimal	<b><math>98.9 \pm 8.1</math></b>	—	—
Sys. 3	Neural Network	p.f.	$5.2 \pm 3.9$	$1.6 \pm 1.1$	$3.1 \pm 1.2$
		<b>p.f. + sub.</b>	<b><math>7.2 \pm 7.2</math></b>	<b><math>2.1 \pm 2.0</math></b>	<b><math>2.6 \pm 1.2</math></b>
Sys. 3	Cold	optimal	$83.6 \pm 5.6$	$25.6 \pm 2.3$	—
		p.f.	$224.6 \pm 22.3$	$68.5 \pm 3.6$	$98.3 \pm 38.9$
Sys. 3	Cold	p.f. + sub.	$255.1 \pm 26.7$	$77.8 \pm 4.6$	$6.4 \pm 3.7$
		optimal	<b><math>327.1 \pm 17.1</math></b>	—	—
Sys. 4	Neural Network	p.f.	$17.4 \pm 7.9$	$1.1 \pm 0.4$	$4.9 \pm 1.5$
		<b>p.f. + sub.</b>	<b><math>27.8 \pm 23.2</math></b>	<b><math>1.7 \pm 1.2</math></b>	<b><math>3.5 \pm 1.6</math></b>
Sys. 4	Cold	optimal	$400.4 \pm 12.9$	$25.0 \pm 2.4$	—
		p.f.	$1074.4 \pm 113.0$	$66.6 \pm 1.8$	$192.9 \pm 53.1$
Sys. 4	Cold	p.f. + sub.	$1262.1 \pm 182.1$	$78.0 \pm 4.4$	$6.3 \pm 3.3$
		optimal	<b><math>1611.7 \pm 139.2</math></b>	—	—

Fig. 7. Test Set Metrics: These metrics report the number of iterations and suboptimality of the the various intialization and temrmination methods on the 4 systems. Our method is displayed in magenta, and the baseline method is displayed in olive.

ria must be met in order to obtain good performance. This discrepancy demonstrates that the neural network alone is obtaining a good guess in terms of the objective function, and the iterations serve mostly as slight modifications to obtain satisfaction of the constraints and suboptimality criteria.

For the low dimensional Sys. 1, the suboptimality level of both the neural network and cold start methods when only primal feasibility is achieved is very high. The reason for this anomaly is that these systems have many examples where the optimal objective function is close to 0, so the presentation as a percentage to the optimal objective appears very high. Practically it is not significant, as only a few iterations ( $\sim 6$ ) are needed to reach the suboptimality criteria for this system.

#### 9.4 Scaling Metrics

There are a variety of challenges related to scaling to a high dimensional system. We highlight two here that have shaped our approach. The first is in how we provide guarantees, and the second is in how we generate the train and test data sets.

Our approach to provide guarantees on the RHC is to utilize an online primal active set solver, but an alternative method that provides statistical guarantees is to look at the performance of only the neural network on a test set. These statistical guarantees can be provided by obtaining primal feasibility and suboptimality certificates on all of the samples in the test set [15, 41] using only the neural network. This approach is appealing since it is a completely explicit approach. However, we find that for large systems, it is extremely challenging, if not impossible, to obtain these certificates for a method



that only uses a neural network.

Our neural network outputs a primal feasible prediction for 61.6% of the samples in the test set for the low-dimensional Sys. 1. However, for all the remaining larger systems, 0% of the samples in the test set are primal feasible. As a result, the output of a a neural networks without additional active set iterations will almost never satisfy the primal feasibility criteria for all the examples in the test set to provide a statistical guarantee. These results are more surprising because they seemingly contradict the other high performing train and test metrics.

The intuition behind this is that for constrained optimization problems like mp-QP, the optimal solution will typically lie on the boundary of the constrained region. The number of boundaries correspond to the number of active constraints in the optimal working set  $\mathcal{W}_A^*$ . For a network output to be primal feasible, it must satisfy all of these constraints. Assuming that the network output is a random variable where the mean is centered at the optimal primal variable, and the variance is fixed regardless of the number of active sets, the probability that it satisfies all of the active constraints quickly goes to 0 as the number of active constraints increases because violating any constraint will make it primal infeasible. This behavior will occur even if the network output is close to optimal, but happens to lie slightly on the wrong side of one of the active constraints.

The second challenge to scaling to a large system is the data generation process, which we discussed in Sec. 8. Obtaining good generalization on a high-dimensional system requires a large data set. However, without an efficient data set generation strategy, it would be impractical to obtain this large data set to train the neural network. The naive method to generating a data set is through rejection sampling. Fig. 8 shows that the percentage of sampled states that are feasible quickly approaches 0 for large systems such as Sys. 4. Considering from Fig. 6 that the cold *optimal* method takes 336 ms to solve 1 problem instance, and that Fig. 8 shows that only 0.4% of sampled states will be feasible, a rough calculation shows that generating a dataset of 1M feasible states will take 2.6 *years*. This simple calculation highlights how important it is to design a specialized data set generation algorithm such as our proposed method.

Fig. 2 shows the dataset sizes and computation time from our proposed dataset generation algorithm. For the large Sys. 4, our algorithm was able to generate a dataset of 1.7M feasible states in 5.2 hours, much smaller than the hypothetical 75 days it would take using rejection sampling with 32 parallel processes. Our proposed data set generation algorithm is faster both because it is more efficient in finding feasible states, but also because it can utilize hot starts and solve a sequence of closely related problems. For Sys. 4, this speedup is approximately  $4.5\times$

System	Rejection Sampling Feasible Percentage
Sys. 1	98.6%
Sys. 2	16.7%
Sys. 3	1.1%
Sys. 4	0.4%

Fig. 8. Rejection sampling does not scale to large systems.

as shown in comparing the cold *optimal* and hot *optimal* in Fig. 6.

## 10 Conclusion

We presented a hybrid explicit-implicit MPC procedure that combines an offline trained neural network with an online primal active set solver. The neural network component allows our approach to scale to high dimensional problems, while the primal active set solver provides corrective steps to meet the conditions necessary to provide guarantees on recursive feasibility and asymptotic stability. Our numerical results demonstrate that our approach scales to large problems including one with 36 states, 9 inputs, and time horizon of 50.

We highlighted the close relationship between mp-QP and ReLu DNN which justified our choice of restricting our planner to the functions computed by ReLu DNN. We proposed a primal-dual loss function based on the Lagrangian to train the neural network. We derived an algorithm to provide certificates of primal feasibility and suboptimality, the criteria necessary to guarantee recursive feasibility and asymptotic stability, based on the approximation of the primal variables only. Finally, we show how the concepts of warm starting and early termination can be used to combine the primal active set solver with the neural network to accelerate inference times.

The key challenge of function approximation in high dimensional mp-QP is choosing good training points in a convex set defined by a membership oracle. We introduced ideas from *geometric random walks* and *QMC* sequences through an algorithm that can efficiently generate large dataset for large problems. Our results indicate the importance of addressing this problem in order to obtain a scalable solution.

## Acknowledgements

This work is supported in part by ARO grant W911NF-13-1-0350, DARPA grant HR001151626/HR0011516850, NSF CRII RI IIS-1755568, the Semiconductor Research Corporation (SRC), and the NVIDIA AI Labs program.

## References

- [1] Martín Abadi, Paul Barham, Jianmin Chen, Zhifeng Chen, Andy Davis, Jeffrey Dean, Matthieu Devin, Sanjay Ghemawat, Geoffrey Irving, Michael Isard, et al. Tensorflow: a system for large-scale machine learning. In *OSDI*, volume 16, pages 265–283, 2016.
- [2] Ilya A Antonov and VM Saleev. An economic method of computing  $l_p$ -sequences. *USSR Computational Mathematics and Mathematical Physics*, 19(1):252–256, 1979.
- [3] Raman Arora, Amitabh Basu, Poorya Mianjy, and Anirbit Mukherjee. Understanding deep neural networks with rectified linear units. In *International Conference on Learning Representations*, 2018.
- [4] Alberto Bemporad, Manfred Morari, Vivek Dua, and Efstratios N Pistikopoulos. The explicit linear quadratic regulator for constrained systems. *Automatica*, 38(1):3–20, 2002.
- [5] Francesco Borrelli, Alberto Bemporad, and Manfred Morari. *Predictive control for linear and hybrid systems*. Cambridge University Press, 2017.
- [6] Patrick Bouffard, Anil Aswani, and Claire Tomlin. Learning-based model predictive control on a quadrotor: Onboard implementation and experimental results. In *IEEE Int. Conf. on Robotics and Automation (ICRA)*, pages 279–284, 2012.
- [7] Stephen Boyd and Lieven Vandenberghe. *Convex optimization*. Cambridge university press, 2004.
- [8] Steven Chen, Kelsey Saulnier, Nikolay Atanasov, Daniel D Lee, Vijay Kumar, George J Pappas, and Manfred Morari. Approximating explicit model predictive control using constrained neural networks. In *2018 Annual American Control Conference (ACC)*, pages 1520–1527. IEEE, 2018.
- [9] Tom Erez, Kendall Lowrey, Yuval Tassa, Vikash Kumar, Svetoslav Kolev, and Emanuel Todorov. An integrated system for real-time model predictive control of humanoid robots. In *IEEE Int. Conf. on Humanoid Robots*, pages 292–299, 2013.
- [10] H.J. Ferreau, H.G. Bock, and M. Diehl. An online active set strategy to overcome the limitations of explicit mpc. *International Journal of Robust and Nonlinear Control*, 18(8):816–830, 2008.
- [11] Philip E. Gill, Walter Murray, Michael A. Saunders, and Elizabeth Wong. User’s guide for SQOPT 7.7: Software for large-scale linear and quadratic programming. Center for Computational Mathematics Report CCoM 18-2, Department of Mathematics, University of California, San Diego, La Jolla, CA, 2018.
- [12] Ian Goodfellow, Yoshua Bengio, and Aaron Courville. *Deep Learning*. MIT Press, 2016. <http://www.deeplearningbook.org>.
- [13] Boris Hanin and David Rolnick. Deep relu networks have surprisingly few activation patterns. *arXiv preprint arXiv:1906.00904*, 2019.
- [14] M. Herceg, M. Kvasnica, C.N. Jones, and M. Morari. Multi-Parametric Toolbox 3.0. In *Proc. of the European Control Conference*, pages 502–510, Zürich, Switzerland, July 17–19 2013. <http://control.ee.ethz.ch/~mpt>.
- [15] Michael Hertneck, Johannes Kohler, Sebastian Trimpe, and Frank Allgöwer. Learning an approximate model predictive controller with guarantees. PP:1–1, 06 2018.
- [16] Michael Hertneck, Johannes Köhler, Sebastian Trimpe, and Frank Allgöwer. Learning an approximate model predictive controller with guarantees. *IEEE Control Systems Letters*, 2(3):543–548, 2018.
- [17] Juan L Jerez, Paul J Goulart, Stefan Richter, George A Constantinides, Eric C Kerrigan, and Manfred Morari. Embedded online optimization for model predictive control at megahertz rates. *IEEE Transactions on Automatic Control*, 59(12):3238–3251, 2014.
- [18] Elizabeth John and E Alper Yildirim. Implementation of warm-start strategies in interior-point methods for linear programming in fixed dimension. *Computational Optimization and Applications*, 41(2):151–183, 2008.
- [19] Colin N Jones and Manfred Morari. Polytopic approximation of explicit model predictive controllers. *IEEE Trans. on Auto. Control*, 55(11):2542–2553, 2010.
- [20] Kenji Kawaguchi and Yoshua Bengio. Generalization in machine learning via analytical learning theory. *arXiv preprint arXiv:1802.07426*, 2018.
- [21] Diederik P Kingma and Jimmy Ba. Adam: A method for stochastic optimization. *arXiv preprint arXiv:1412.6980*, 2014.
- [22] Martin Klaučo, Martin Kalúz, and Michal Kvasnica. Machine learning-based warm starting of active set methods in embedded model predictive control. *Engineering Applications of Artificial Intelligence*, 77:1–8, 2019.
- [23] Michal Kvasnica and Miroslav Fikar. Clipping-based complexity reduction in explicit mpc. *IEEE Trans. on Auto. Control*, 57(7):1878–1883, 2012.
- [24] Gunther Leobacher and Friedrich Pillichshammer. *Introduction to quasi-Monte Carlo integration and applications*. Springer, 2014.
- [25] Sikang Liu, Nikolay Atanasov, Kartik Mohta, and Vijay Kumar. Search-based motion planning for quadrotors using linear quadratic minimum time control. In *2017 IEEE/RSS International Conference on Intelligent Robots and Systems (IROS)*, pages 2872–2879. IEEE, 2017.
- [26] Daniel Warren Mellinger. Trajectory generation and control for quadrotors. 2012.
- [27] Guido F Montufar, Razvan Pascanu, Kyunghyun Cho, and Yoshua Bengio. On the number of linear regions of deep neural networks. In *Advances in neural information processing systems*, pages 2924–2932, 2014.
- [28] Harald Niederreiter. *Random number generation and quasi-Monte Carlo methods*, volume 63. Siam, 1992.
- [29] S Joe Qin and Thomas A Badgwell. A survey of industrial model predictive control technology. *Control engineering practice*, 11(7):733–764, 2003.
- [30] Charles Richter, William Vega-Brown, and Nicholas Roy. Bayesian learning for safe high-speed navigation in unknown environments. In *Robotics Research*, pages 325–341. Springer, 2018.
- [31] Stéphane Ross, Geoffrey Gordon, and Drew Bagnell. A reduction of imitation learning and structured prediction to no-regret online learning. In *Proceedings of the fourteenth international conference on artificial intelligence and statistics*, pages 627–635, 2011.
- [32] Il’ya Meerovich Sobol’. On the distribution of points in a cube and the approximate evaluation of integrals. *Zhurnal Vychislitel’noi Matematiki i Matematicheskoi Fiziki*, 7(4):784–802, 1967.
- [33] Sean Summers, Colin N Jones, John Lygeros, and Manfred Morari. A multiresolution approximation method for fast explicit model predictive control. *IEEE Transactions on Automatic Control*, 56(11):2530–2541, 2011.

- [34] Tijmen Tieleman and Geoffrey Hinton. Lecture 6.5-rmsprop: Divide the gradient by a running average of its recent magnitude. *COURSERA: Neural networks for machine learning*, 4(2):26–31, 2012.
- [35] Santosh Vempala. Geometric random walks: a survey. *Combinatorial and computational geometry*, 52(573-612):2, 2005.
- [36] Sergey Vichik and Francesco Borrelli. Solving linear and quadratic programs with an analog circuit. *Computers & Chemical Engineering*, 70:160–171, 2014.
- [37] Yang Wang and Stephen Boyd. Fast model predictive control using online optimization. *IEEE Trans. Control Syst. Technol.*, 18(2):267–278, 2010.
- [38] Michael Watterson and Vijay Kumar. Safe receding horizon control for aggressive mav flight with limited range sensing. *IEEE/RSJ Int. Conf. on Intelligent Robots and Systems (IROS)*, pages 3235–3240, 2015.
- [39] Stephen Wright and Jorge Nocedal. Numerical optimization. *Springer Science*, 35(67-68):7, 1999.
- [40] Melanie Nicole Zeilinger, Colin Neil Jones, and Manfred Morari. Real-time suboptimal model predictive control using a combination of explicit mpc and online optimization. *IEEE Transactions on Automatic Control*, 56(7):1524–1534, 2011.
- [41] Xiaojing Zhang, Monimoy Bujarbaruah, and Francesco Borrelli. Safe and near-optimal policy learning for model predictive control using primal-dual neural networks. *2019 American Control Conference (ACC)*, pages 354–359, 2019.